Molecular Biology of the Cell
Vol. 10, 2441–2459, July 1999

Rho-dependent Regulation of Cell Spreading by the Tetraspan Membrane Protein Gas3/PMP22

Claudio Brancolini,*†‡ Stefania Marzinotto,* Paolo Edomi,*§ Elena Agostoni,* Carla Fiorentini,‖ Hans Werner Müller,¶ and Claudio Schneider*†

*Laboratorio Nazionale Consorzio Interuniversitario Biotecnologie, 34142 Trieste, Italy; †Dipartimento di Scienze e Tecnologie Biomediche, Sezione di Biologia-Universitá di Udine, 33100 Udine, Italy; §Dipartimento di Biologia Universitá di Trieste, 34100 Trieste, Italy; ‖Dipartimento di Ultrastruttura, Istituto Superiore di Sanitá, 00161 Rome, Italy; and ¶Molecular Neurobiology Laboratory, Department of Neurology, Heinrich-Heine-University, 40225 Dusseldorf, Germany

Submitted March 2, 1999; Accepted April 23, 1999
Monitoring Editor: Martin Raff

Gas3/PMP22 plays a crucial role in regulating myelin formation and maintenance, and different genetic alterations in *gas3/PMP22* are responsible for a set of human peripheral neuropathies. We have previously demonstrated that Gas3/PMP22 could regulate susceptibility to apoptosis in NIH3T3 cells but not in REF 52 cells. In this report we demonstrate that when the apoptotic response triggered by *gas3/PMP22* was counteracted by Bcl-2 coexpression, morphological changes were observed. Time-lapse analysis confirmed that Gas3/PMP22 can modulate cell spreading, and this effect was strengthened after inhibition of phosphoinositide 3-kinase. Using the active form of the small GTPase RhoA, we have been able to dissect the different Gas3/PMP22 biological activities. RhoA counteracted the Gas3/PMP22-dependent morphological response but was unable to neutralize the apoptotic response. Treatment of NIH3T3 cells with cytotoxic necrotizing factor 1, which activates endogenous Rho, also counteracted Gas3/PMP22-mediated cell shape and spreading changes. Treatment of REF 52 cells, which are unresponsive to Gas3/PMP22 overexpression, with the C3 exoenzyme, inhibiting Rho activity, renders REF 52 cells responsive to Gas3/PMP22 overexpression for cell shape and spreading changes. Finally, assembly of stress fibers and focal adhesions complexes, in response to lysophosphatidic acid–induced endogenous Rho activation, was impaired in Gas3/PMP22-overexpressing cells. We hypothesize that cell shape and spreading regulated by Gas3/PMP22 through the Rho GTPase might have an important role during Schwann cells differentiation and myelinization.

INTRODUCTION

Gas3/PMP22, a member of an extended family of tetraspan membrane proteins (Marvin *et al.*, 1995; Taylor *et al.*, 1995; Bolin *et al.*, 1997; Magyar *et al.*, 1997), is highly expressed in myelinating Schwann cells, where it represents 2–5% of total myelin proteins, largely confined to compact myelin (Spreyer *et al.*, 1991; Welcher *et al.*, 1991; Snipes *et al.*, 1992; Suter and Snipes, 1995). Gas3/PMP22 expression is also induced during growth arrest and apoptosis in fibroblasts (Manfioletti *et al.*, 1990; Brancolini *et al.*, 1997), and it has been detected during mouse development and in adulthood in different neural and non-neural tissues (Baechner *et al.*, 1995; Fabbretti *et al.*, 1995).

Genetic studies (for review, see Patel and Lupski, 1994; Suter and Snipes, 1995) and the generation of *gas3/PMP22*-deficient mice (Adlkofer *et al.*, 1995) have clearly established that *gas3/PMP22* is responsible for a set of inherited peripheral neuropathies in mice and humans. Charcot–Marie–Tooth type 1 (CMT1) disease

‡ Corresponding author. E-mail address: brancoli@sci.area.trieste.it.
Abbreviations used: AK, adenylate kinase; CMT, Charcot–Marie–Tooth; CNF, cytotoxic necrotizing factor; h-TR, human transferrin receptor; LPA, lysophosphatidic acid; PI3K, phosphoinositide 3-kinase; WT, wortmannin.

is a peripheral neuropathy characterized by progressive distal muscle weakness and atrophy and impaired sensation of the limbs. The most common form of CMT1 disease, CMT1A, is characterized by genomic duplication on 17p11.2-p12 containing the *gas3/PMP22* locus (Lupski *et al.*, 1991; Matsunami *et al.*, 1992; Patel *et al.*, 1992; Timmerman *et al.*, 1992; Valentijn *et al.*, 1992b). Deletion of the same region is responsible for hereditary neuropathy with liability to pressure palsies (Chance *et al.*, 1993). Further detection of point mutations in the *gas3/PMP22* gene in nonduplication CMT1A families (Valentijn *et al.*, 1992a; Roa *et al.*, 1993b) and in the related severe congenital hypertrophic neuropathy Dejerine–Sottas syndrome (Roa *et al.*, 1993a) confirmed *gas3/PMP22* as disease gene.

If genetic studies hallmark a critical role of *gas3/PMP22* in the formation and maintenance of the myelin envelope, its widespread expression suggests a more general biological function (Suter *et al.*, 1994).

Data from culture overexpression studies indicate a role of *gas3/PMP22* in regulating cell growth. Retroviral *gas3/PMP22* transfer in cultured Schwann cells underlined a growth-suppressive function (Zoidl *et al.*, 1995), and ectopic expression in NIH3T3 fibroblasts was associated with an apoptotic response (Fabbretti *et al.*, 1995; Zoidl *et al.*, 1997). Interestingly, in the last case when *gas3/PMP22* point mutants associated with CMT1A were similarly overexpressed the apoptotic response was reduced and behaved as dominant negatives when coexpressed with the wild-type *gas3/PMP22* (Fabbretti *et al.*, 1995).

In this report we have analyzed the apoptotic response triggered by *gas3/PMP22* overexpression, and we have observed that when the apoptotic response was counteracted, overexpression of *gas3/PMP22* could still induce alterations of cell shape and spreading, which are counteracted by the small GTPase RhoA (for review, see Van Aelst and D'Souza-Schorey, 1997; Hall, 1998). These results confirm the role of Gas3/PMP22 in triggering cell death and unveil a second function in controlling cell morphology, possibly trough the modulation of Rho small GTPase.

MATERIALS AND METHODS

Culture Conditions

NIH3T3 and Swiss 3T3 cells were grown in Dulbecco's modified Eagle's medium supplemented with 10% FCS, penicillin (100 U/ml), and streptomycin (100 μg/ml).

For serum starvation, medium was changed to 0.1% FCS when cells were subconfluent; cells were then left in this medium for 36 h. Lysophosphatidic acid (LPA; Sigma, St. Louis, MO) was used at a final concentration of 70 μM in medium containing 0.1% FCS.

Rat Schwann cells were prepared from the sciatic nerves of neonatal Wistar rats (Brockes *et al.*, 1979). Purified Schwann cells were grown in Dulbecco's modified Eagle's medium supplemented with 10% FCS and 2 μM forskolin for a limited period.

For microinjection assays, cells were grown on coverslips in 35-mm Petri dishes containing 8×10^4 cells per dish. After a 24-h incubation at 37°C in 5% CO_2 atmosphere, cells were microinjected with the appropriate expression plasmid.

Cytotoxic necrotizing factor 1 (CNF1; 1 μg/ml final concentration), purified as previously described (Fiorentini *et al.*, 1997) was added to the culture medium after microinjection. z-Val-Ala-Asp-.fluoromethylketone was obtained from Bachem (Bubendorf, Switzerland). Stock solutions in DMSO were stored at −80°C and used at 100 μM final concentration. Wortmannin (WT) and LY294002 were used, respectively, at 1.33 and 13.3 μM final concentrations.

Microinjection and Time Lapse

Nuclear microinjection was performed using the Automated Injection System (Zeiss, Oberkochen, Germany) as previously described (Fabbretti *et al.*, 1995). Nuclei of the cells were injected with the different expression vectors for 0.5 s at the constant pressure of 150 hectopascal. For time-lapse analysis cells were directly plated on the Petri dishes on which squares of ~4 mm^2 were marked. After microinjection of pGDSV7*gas3/PMP22* or pGDSV7*bax* in the nucleus of growing NIH3T3 cells, the coordinates of the injected cells were stored on a computer disk (Brancolini *et al.*, 1995). Microinjected cells were grown for a further 10 h at 37°C in 5% CO_2 atmosphere and time-lapse series were collected for 22 h at 1-h intervals. During intervals cells were incubated at 37°C in 5% CO_2 atmosphere.

Immunofluorescence Microscopy

For indirect immunofluorescence microscopy, microinjected NIH3T3 cells were fixed with 3% paraformaldehyde in PBS for 20 min at room temperature. Fixed cells were washed with PBS and 0.1 M glycine, pH 7.5, and then permeabilized with 0.1% Triton X-100 in PBS for 5 min. The coverslips were treated with the different first antibodies: anti-hGAS3/PMP22 (Fabbretti *et al.*, 1995), anti-Gas2 (Brancolini *et al.*, 1995), anti-hTR OKT-9, anti-FLAG (Sigma), and anti-P_0 (Archelos *et al.*, 1993), diluted in PBS and 3% BSA for 1 h in a moist chamber at 37°C. They were then washed with PBS three times, followed by incubation with the relative secondary antibodies: FITC-conjugated anti-mouse (Sigma), TRITC-conjugated anti-mouse (Southern Biotechnology, Birmingham, AL), TRITC-conjugated anti-rabbit (Dako, Glostrup, Denmark), and FITC-conjugated anti-rabbit (Sigma), for 1 h at 37°C. Cells were examined by epifluorescence with a Zeiss Axiovert 35 microscope or a Zeiss laser scan microscope (LSM 410) equipped with a 488 λ argon laser and a 543 λ helium neon laser

Survival Assay

The effect on cell survival of different genes was analyzed using an automated injection system. For each experiment an established number of cells (200) was microinjected with the gene of interest and a reporter gene. Cell survival was calculated as the number of recovered cells expressing the reporter gene. All cDNAs were cloned in the same expression vector (Brancolini *et al.*, 1995) and microinjected in NIH3T3 cells. When the pGDSV7-*h-TR* was used as reporter, it was injected at the concentration of 25 ng/μl.

Statistical significance was determined for all data by using one-way analysis of variance (F test); in the case of multiple comparisons the Student–Neuman–Keuls test (q test) was then applied.

Plasmid Construction

Human *gas3/PMP22* cDNA (Edomi *et al.*, 1993) was subcloned in frame with a C-terminal FLAG (Gas3/PMP22-FLAG) in pGDSV7-FLAG. The *hgas3/PMP22* cDNA was amplified by PCR using a sense primer (5′-GAGTGAATTCAACTCCGCTGAGCAGAACTT-3′) containing an *Eco*RI site and a reverse primer containing a *Hin*dIII site (5′-CGCAAGCTTTTCGCGTTTCCGCAAGATCA-3′).

The pGDSV7-FLAG vector was created by inserting an oligonucleotide cassette for the FLAG peptide (DYKDDDDK) in the pGDSV7 vector (Brancolini *et al.*, 1995).

All constructs generated were sequenced using an automated laser fluorescence system to check for the translating fidelity of the inserted PCR fragments.

The *crmA* cDNA was excised from plasmid pDX10 (Xue and Horvitz, 1995) and cloned as *Not*I–*Hin*dIII fragment into pGDSV7. The *bax* cDNA (Oltvai *et al.*, 1993) was excised from pSK as an *Eco*RI fragment and subcloned into the *Eco*RI site of pGDSV7. The cDNAs encoding Bcl-2 (Brancolini *et al.*, 1995), the P_0 protein (Lemke *et al.*, 1988), and adenylate kinase (AK) were subcloned into the *Eco*RI site of the pEXV vector (Ridley *et al.*, 1992).

RESULTS

Apoptosis and Morphological Changes Induced by gas3/PMP22 Overexpression in NIH3T3 Cells

To dissect the apoptotic response triggered by overexpression of *gas3/PMP22* in NIH3T3 cells we decided to study whether well-characterized apoptotic antagonists such as the proto-oncogene *bcl-2* (Reed, 1997) and the cowpox virus gene *crmA* (cytokine response modifier A), which encodes a caspase inhibitor (Cohen, 1997), were able to block cell death as elicited by *gas3/PMP22*.

Apoptosis can be easily monitored and assessed by analyzing cell survival. We used a microinjection-based assay to score cell survival in response to both overexpression of apoptotic genes and the presence of apoptotic stimuli (see MATERIALS AND METHODS).

We first analyzed the antiapoptotic activity of *bcl-2* and *crmA* in NIH3T3 cells deprived of serum. *bcl-2*, *crmA*, and two different controls, *gas2* and human placental alkaline phosphatase (*hPLAP*) (100 ng/μl), were coexpressed with the human transferrin receptor (*h-TR*) as reporter gene (25 ng/μl). Six hours after microinjection apoptosis was induced by serum deprivation, and 16 h later cells were fixed for immunofluorescence analysis. Cell survival was scored as number of recovered cells positive for h-TR.

In cells coexpressing the control genes *gas2* and *hPLAP*, recovery of h-TR-positive cells after induction of apoptosis by complete serum deprivation was impaired with a survival rate of 31 $\pm$ 9–33 $\pm$ 5% (Figure 1A). In contrast, survival was dramatically increased in cells coexpressing *bcl-2/h-TR* with 90 $\pm$ 15% of survival rate ($p < 0.05$). Coexpression of *crmA* less efficiently counteracted apoptosis with respect to *bcl-2*; in fact survival rate was 55 $\pm$ 6.5% ($p < 0.05$).

Having demonstrated the antiapoptotic activity of Bcl-2 and CrmA in our cellular system we next assessed the protective effects of both *crmA* and *bcl-2* on cells overexpressing *gas3/PMP22*.

gas3/PMP22 was coexpressed with *bcl-2*, *crmA*, or different control genes by nuclear microinjection. Cells were grown for further 24 h in 10% FCS and then scored for Gas3/PMP22 expression using anti-Gas3/PMP22 antibody, by immunofluorescence analysis.

The survival rate of microinjected cells coexpressing *gas3/PMP22* and the different control genes was 17 $\pm$ 2.5%. Coexpression of either *bcl-2* or *crmA* significantly added to the number of Gas3/PMP22 expressing cells recovered, thus increasing the survival rate, respectively, to 37 $\pm$ 6 or 28.5 $\pm$ 5% ($p < 0.05$) (Figure 1B). Similar increased survival rates (27 $\pm$ 5%) in cells overexpressing Gas3/PMP22 were also obtained when a broad-spectrum cell-permeable caspase inhibitor, the benzyloxycarbonyl-Val-Ala-Asp.fluoromethylketone (McCarthy *et al.*, 1997), was used (our unpublished results).

Having demonstrated that *gas3/PMP22* overexpression leads to an apoptotic response inhibited by Bcl-2, the next step was to compare the Gas3/PMP22 apoptotic activity with that of a well-known killer gene such as *bax*. Bax is a proapoptotic member of the Bcl-2 protein family (Oltvai *et al.*, 1993; Green and Kroemer, 1998; Silke and Vaux, 1998).

NIH3T3 fibroblasts were injected with *h-TR*, as reporter gene, and with increasing amounts of *gas3/PMP22* or the killer gene *bax* (Figure 1C). *bax* reduced survival rates to 66 $\pm$ 1% when coexpressed at a concentration of 25 ng/μl, and full killer activity was detected at 100 ng/μl (survival rate, 4 $\pm$ 1.5%).

gas3/PMP22 when coexpressed at concentration of 25 ng/μl reduced the survival rate to 74.5 $\pm$ 3%, and its killer activity constantly increased at higher coexpression dosages, reaching a survival rate of 13.5 $\pm$ 2% at a concentration of 150 ng/μl. When *h-TR* was coexpressed with an increasing amount of the control gene *gas2*, survival rates were ~100% (Figure 1C).

In summary, even though *gas3/PMP22* and *bax* showed an overall similar dose-dependent killer activity, when measured as survival rates, *bax* was more active in triggering cell death than *gas3/PMP22*.

When a detailed analysis of the cell morphology was performed in Gas3/PMP22- and Bcl-2-coexpressing cells, it was evident that relative to the increased recovery of Gas3/PMP22-overexpressing cells a significant fraction of them showed peculiar morphological changes (see the next sections for the quantitative analysis). As shown in Figure 1D, B, NIH3T3 cells coexpressing h-TR and Bcl-2 presented a normal phenotype, cells appearing well spread and nuclei regular. On the contrary, cells coexpressing Gas3/PMP22 and Bcl-2 showed a peculiar phenotype. In these cells spreading was apparently reduced, some thin cellular processes could be observed, and nuclei maintained their overall normal morphology without evident markers of fragmentation (Figure 1D, A).

Several mutations in the P_0 gene, which encodes for another component of the compact myelin, have been found, and the resulting phenotypes were clinically classified as CMT1B or Dejerine–Sottas syndrome (for review, see Suter and Snipes, 1995). Therefore, we analyzed whether similar morphological changes were induced in NIH3T3 cells after overexpression of P_0. Despite the mutual involvement of *gas3/PMP22*

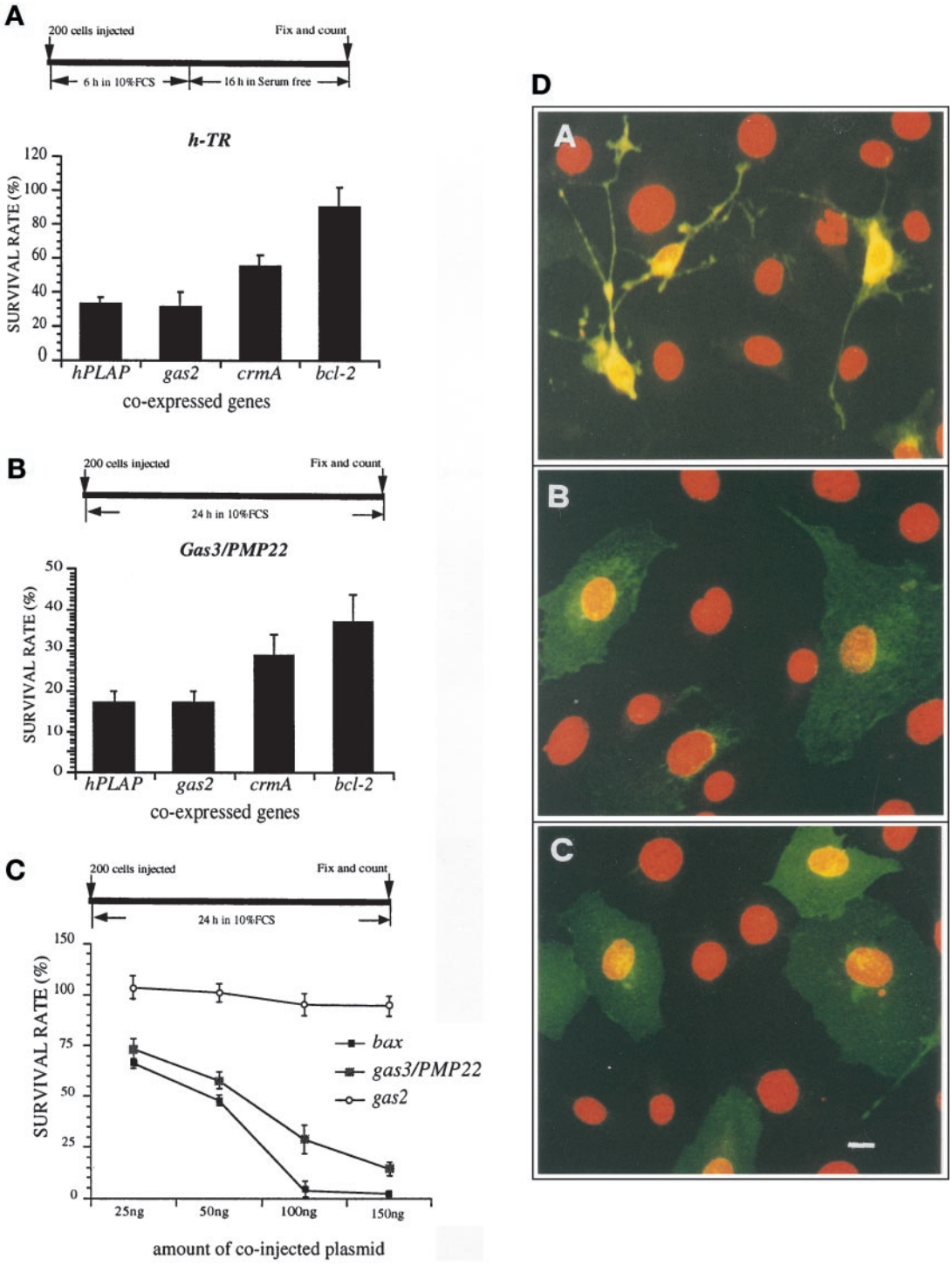

Figure 1. bcl-2 counteracts apoptosis induced by gas3/PMP22. (A) *bcl-2*, *crmA*, *gas2*, and *hPLAP* were coexpressed with *h-TR* in NIH3T3 cells. Six hours after microinjection apoptosis was induced by serum deprivation. Sixteen hours later cells were fixed and processed for immunofluorescence to detect h-TR. Survival was scored as described in the text. Data represent arithmetic means ± SD for five independent experiments ($p < 0.001$). (B) *bcl-2*, *crmA*, *gas2*, and *hPLAP* were coexpressed with *gas3/PMP22* in NIH3T3 cells. After 24 h from microinjection cells were fixed and processed for immunofluorescence to detect Gas3/PMP22. Survival was scored as described in the text. Data represent arithmetic means ± SD for five independent experiments ($p < 0.001$). (C) *gas3/PMP22* and *bax* killer activity. Different amounts of pGDSV7S containing *gas3/PMP22*, *bax*, or *gas2* were comicroinjected with pGDSV7*h-TR* (25 ng/μl) in the nuclei of NIH3T3 cells. After 24 h from microinjection cells were fixed and processed for immunofluorescence to detect h-TR. Survival was scored as described in the text. Data

and P_0 in generating peripheral neuropathies, overexpression of P_0 was unable to induce morphological changes in NIH3T3 cells (Figure 1D, C).

The described altered phenotype could be dependent on a delayed apoptotic response or on a second biological activity of Gas3/PMP22, which could become more evident in the presence of Bcl-2. This observation prompted us to investigate whether Gas3/PMP22 could play a role also in regulating morphological changes.

Overexpression of Gas3/PMP22 in Schwann Cells Triggers Apoptosis and Cell Shape Changes

Gas3/PMP22 is abundantly expressed in myelinating Schwann cells, and different genetic alterations involving Gas3/PMP22 are responsible for different peripheral neuropathies. Having demonstrated a role of Gas3/PMP22 in regulating apoptosis and possibly morphological changes in NIH3T3 fibroblasts, we next analyzed whether similar biological activities could be observed also after its overexpression in highly purified rat Schwann cells (Zoidl *et al.*, 1995).

Schwann cells were microinjected with pGDSV7-*hgas3/PMP22,* fixed 24 h later, and processed for immunofluorescence analysis to detect Gas3/PMP22. A reduced number of Schwann cells overexpressing Gas3/PMP22 were recovered with respect to h-TR-overexpressing cells used as a control, thus suggesting a reduced cell survival (our unpublished results). In addition, some Gas3/PMP22-overexpressing cells showed apoptotic features such as a collapsed cellular body and nuclear fragmentation, whereas h-TR-overexpressing Schwann cells showed a normal phenotype (Figure 2A).

To confirm the induction of an apoptotic phenotype after Gas3/PMP22 overexpression in Schwann cells, *gas3/PMP22* was coexpressed with *bcl-2* or with *h-TR* as control gene. Cells were grown for further 24 h in 10% FCS and then scored for Gas3/PMP22 expression using anti-Gas3/PMP22 antibody.

The survival rate of the microinjected cells coexpressing *gas3/PMP22* and the *h-TR* was ~18 ± 1.7%. In contrast, survival was increased in Schwann cells coexpressing *gas3/PMP22* and *bcl-2*, with ~48 ± 3.3% of survival rate (Figure 2B).

We next analyzed cell morphology of Schwann cells coexpressing Gas3/PMP22 and Bcl-2. For this purpose *gas3/PMP22* (50 ng/μl), *bcl-2* (50 ng/μl), and *gas2* (25 ng/μl), used as reporters, were comicroinjected in Schwann cells, and as a control *h-TR* (50 ng/μl), *bcl-2* (50 ng/μl), and *gas2* (25 ng/μl) were coexpressed. Double immunofluorescence was performed to visualize Gas2 and actin filaments. As shown in Figure 2C, Schwann cells coexpressing, h-TR Bcl-2, and Gas2 presented a normal phenotype; on the contrary, Schwann cells coexpressing Gas3/PMP22 Bcl-2 and Gas2 showed an altered phenotype. As described above for NIH3T3 fibroblasts, cell spreading was apparently reduced, and some thin cellular processes could be observed (Figure 2C, arrowheads).

In summary, Schwann cells respond to Gas3/PMP22 overexpression, showing a reduced survival and a specific morphological response, as reported above for NIH3T3 fibroblasts. These results differ from a previously reported growth-suppressing function of Gas3/PMP22 in cultured Schwann cells using retroviral-mediated gene transfer (Zoidl *et al.*, 1995). This discrepancy probably reflects the distinct methodological approaches applied in these studies, which lead to different levels of Gas3/PMP22 expression and different times of analysis.

Time-Lapse Observation of the Morphological Changes in Living gas3/PMP22-overexpressing Cells

From the previous analysis it was clear that primary Schwann cells and NIH3T3 fibroblasts respond similarly to Gas3/PMP22 overexpression in terms of both cell death and morphological changes. To observe the appearance, development, and dynamics of *gas3/PMP22*-induced morphological changes in living cells and to discriminate between the apoptotic and the morphological responses, we decided to perform a time-lapse analysis. Because Schwann cells and NIH3T3 fibroblasts respond similarly to Gas3/PMP22 overexpression, we decided to use NIH3T3 cells for this analysis.

Figure 3 shows views of a typical cell overexpressing *gas3/PMP22* (arrow). Fifteen hours after microinjection some changes on cell morphology can be observed. A *gas3/PMP22*-overexpressing cell reduced spreading on the substratum, and this process slowly evolved until 22 h after microinjection. Between 22 and 23 h the cell became rounded, and a thin process reminiscent of the adhesion area was detectable. After this time the cell maintained this morphology, with a slight decrease in size, until 28 h when membrane blebbing was evident, indicating a switch to apoptosis.

When the same analysis was performed for a *bax*-overexpressing cell, the emerging picture was different. As shown in Figure 4, a *bax*-overexpressing cell (arrow) showed a normal phenotype until 18 h from

Figure 1 (cont). represent arithmetic means ± SD for three independent experiments. (D) gas3/PMP22-dependent morphological changes: confocal generated overlay showing cellular and nuclear phenotypes in NIH3T3 cells coexpressing Gas3/PMP22 and Bcl-2 (A) or h-Tr and Bcl-2 (B) or P_0 (C). NIH3T3 cells 24 h after seeding were microinjected with pGDSV3-*hTR* (100 ng/μl) and pGDSV7-*bcl-2* (50 ng/μl), with pGDSV7-*gas3/PMP22* (100 ng/μl) and pGDSV7-*bcl-2* (50 ng/μl), or with pEXV-P_0 (100 ng/μl). After 24 h cells were fixed and processed for immunofluorescence analysis to visualize Gas3/PMP22 (dA), h-TR (dB), or P_0 (dC) (green) using the specific antibodies. Propidium iodide was used to visualize nuclei (red). Images were overlayered using a Zeiss confocal microscope and are displayed in pseudocolor. Bar, 5 μm.

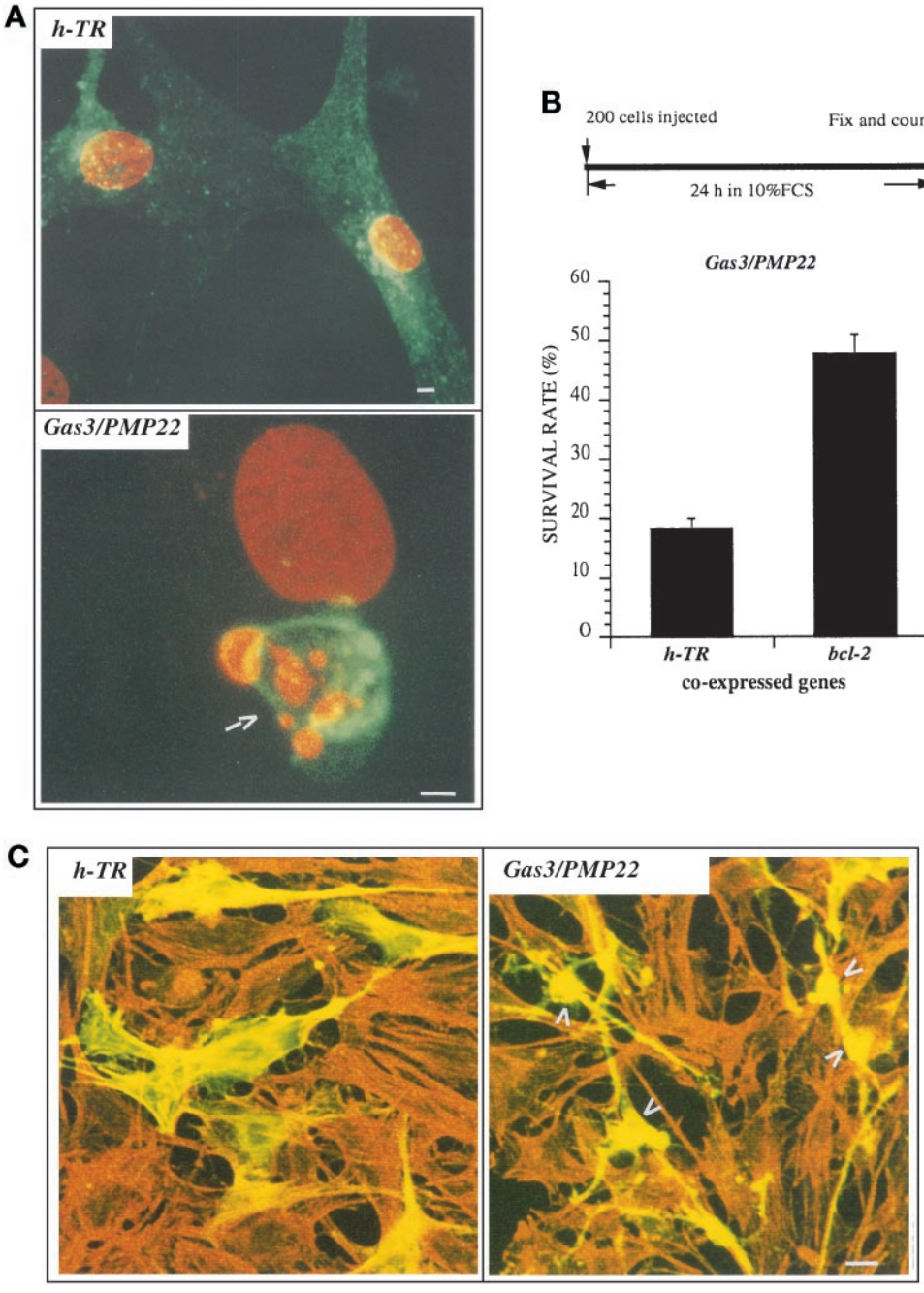

Figure 2. gas3/PMP22-dependent biological activities in Schwann cells. (A) Confocal generated overlay showing nuclear morphology in rat Schwann cells overexpressing Gas3/PMP22 or h-TR. Schwann cells 24 h after seeding were microinjected with pGDSV7-*gas3/PMP22* (100 ng/μl) or with pGDSV3-*hTR* (100 ng/μl); after 24 h cells were fixed and processed for immunofluorescence analysis to visualize Gas3/PMP22 or h-TR using the specific antibodies (green). Propidium iodide was used to visualize nuclei (red). Images were overlayered using a Zeiss confocal microscope and are displayed in pseudocolor. The arrow indicates a Gas3/PMP22-overexpressing cell. Bar, 5 μm. (B) *bcl-2* and *h-TR* were coexpressed with *gas3/PMP22* in Schwann cells. After 24 h from microinjection cells were fixed and processed for immunofluorescence to detect Gas3/PMP22. Survival was scored as described in the text. Data represent arithmetic means ± SD for five independent experiments ($p < 0.001$). (C) Confocal generated overlay showing actin architecture and cell morphology in Schwann cells cells coexpressing Gas3/PMP22 Bcl-2 and Gas2 or h-Tr Bcl-2 and Gas2. Schwann cells 24 h after seeding were microinjected with pGDSV3-*hTR* (50 ng/μl), pGDSV7-*bcl-2* (50 ng/μl), and pGDSV7-*gas2* (25 ng/μl) or with pGDSV7-*gas3/PMP22* (50 ng/μl), pGDSV7-*bcl-2* (50 ng/μl), and pGDSV7-*gas2* (25 ng/μl). After 24 h cells were fixed and processed for immunofluorescence analysis to visualize Gas2 (green), using the specific antibody and actin filaments (red) and rhodamine-phalloidin. Images were overlayered using a Zeiss confocal microscope and are displayed in pseudocolor. Bar, 15 μm.

microinjection. At 19 h membrane blebbing was evident, indicating activation of the apoptotic process. This behavior is in aggreement with a previously reported analysis in fibroblastic cells (McCarthy *et al.*, 1997) in which apoptosis, in terms of morphological events, was described as a process that typically takes between 30 and 60 min. Therefore, in the *bax*-overexpressing cells no specific morphological changes anticipating the appearance of membrane blebbing, as in the case of *gas3/PMP22*, were observed.

This analysis suggested that *Gas3/PMP22* overexpression in NIH3T3 cells leads to both drastic alteration of cell morphology characterized by reduced spreading and retraction from adhesion area, and cell death by apoptosis.

Morphological Changes but Not Apoptosis Can Be Counteracted by Overexpression of Active RhoA

The Rho family of GTP-binding proteins have been implicated in different biological activities (for review,

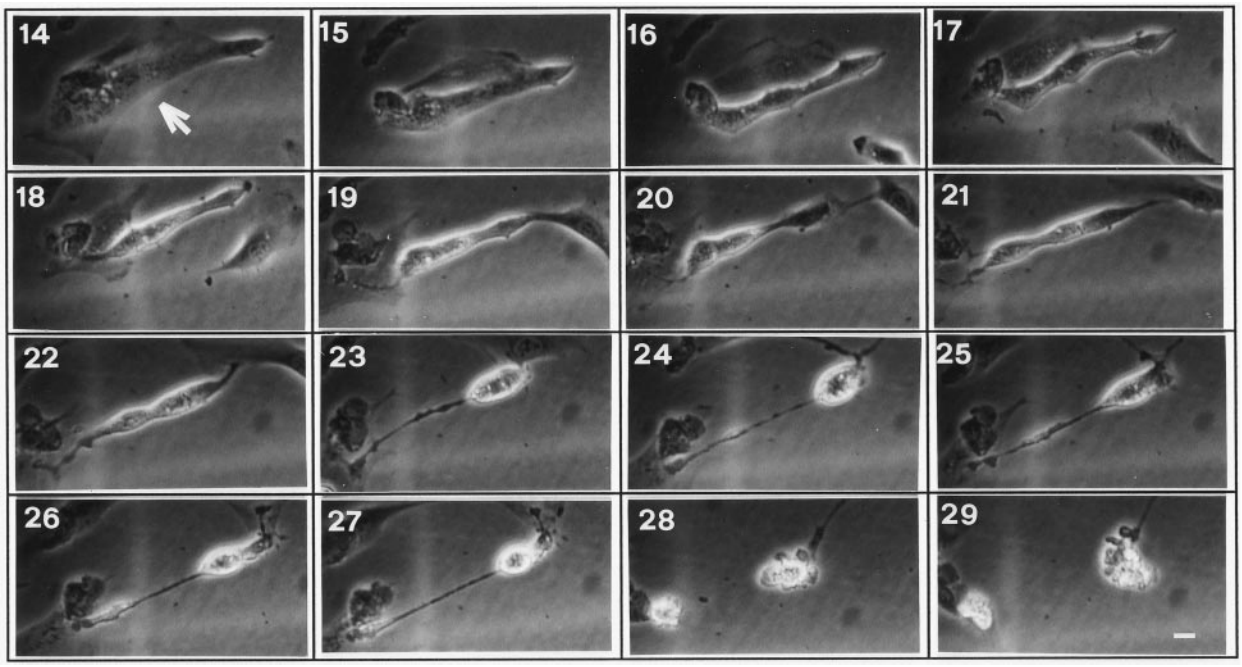

Figure 3. Time-lapse images of a NIH3T3 cell overexpressing gas3/PMP22. Representative cell (arrow) injected with pGDSV7-*gas3/PMP22* (100 ng/μl). Pictures at selected times after microinjection (as indicated) show the morphological changes from 17 h and the appearance of membrane blebbing at 28 h. Bar, 20 μm.

see Van Aelst and D'Souza-Schorey, 1997; Hall, 1998) and more specifically the organization of the actin cytoskeleton and the formation/maintenance of focal adhesion, the sites where stress fibers are linked via integrins to the extracellular matrix (Ridley and Hall, 1992; Machesky and Hall, 1996). Having identified a putative function of Gas3/PMP22 in regulating cell shape and spreading, we decided to analyze whether the constitutively active form of RhoA (RhoA-V14) was able to interfere with the morphological changes induced by *gas3/PMP22* overexpression.

gas3/PMP22FLAG was coexpressed by nuclear microinjection in NIH3T3 cells together with *rhoA*-V14 or with *AK* as control gene. All the cDNAs were cloned in the same expression vector and microinjected, respectively, at the concentrations of 100 ng/μl (*gas3/PMP22FLAG*) and 25 ng/μl (*AK* and *rhoA*-V14). Cells were grown for further 24 h in 10% FCS and then scored both for Gas3/PMP22 expression and for morphological changes by immunofluorescence analysis.

To analyze the Gas3/PMP22-specific morphological changes, therefore excluding cells in apoptosis, only cells that presented reduced spreading sometimes with thin elongated processes (Figure 5B), but without apoptotic markers such as membrane blebbing and evident nuclear fragmentation, were considered for this analysis.

When compared with the survival rates reported above (Figure 1B) overexpression of *gas3/PMP22FLAG* showed reduced killer activity (~27 ± 8% survival rate compared with the ~17 ± 2.5% of the previous experiments). Such a discrepancy was dependent on the different detection system used for the immunofluorescence analysis. In fact, the antibody against the FLAG epitope allowed us also to score cells expressing lower levels of Gas3/PMP22, which were undetectable using the antibody against Gas3/PMP22. This effect has been clearly demonstrated by performing a double immunofluorescence analysis in cells overexpressing Gas3/PMP22FLAG using both antibodies against the FLAG or Gas3/PMP22 (our unpublished results).

Cell survival was not appreciably increased in cells coexpressing *rhoA*V14; in fact, the survival rate was ~32 ± 7%, similar to the survival rate of ~27 ± 8% observed after coexpression of the control gene *AK* (Figure 5A).

Instead, a marked difference was observed for the number of cells showing altered shape. Coexpression of *rhoA*-V14 induced a clear suppression of the Gas3/PMP22-dependent cell shape and spreading changes described above, with 10 ± 1.4% of the cells showing altered morphology in comparison with 37 ± 3.5% of the cells when the control gene was coexpressed (Figure 5A). In Figure 5B representative fields of cells coexpressing *gas3/PMP22FLAG* and *AK* or *rhoA*-V14 as detected after immunofluorescence analysis are reported.

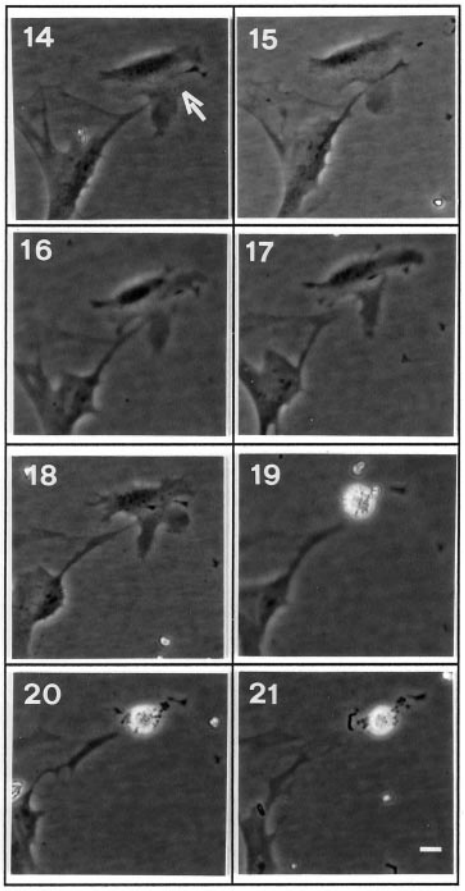

Figure 4. Time-lapse images of an NIH3T3 cell overexpressing bax. Representative cell (arrow) injected with pGDSV7-*bax* (50 ng/μl). Pictures at selected times after microinjection (as indicated) show the appearance of membrane blebbing at 19 h. Bar 20 μm.

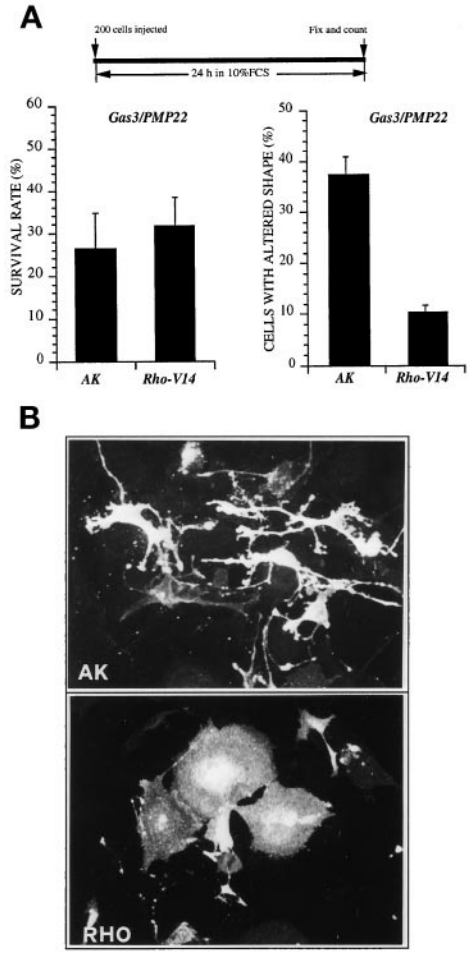

Figure 5. Coexpression of Gas3/PMP22 and RhoA-V14 in NIH3T3 cells. (A) *AK* and *rhoA*-V14 were coexpressed with *gas3/PMP22* in NIH3T3 cells. After 24 h from microinjection cells were fixed and processed for immunofluorescence to detect Gas3/PMP22FLAG. Survival and morphological changes were scored as described in the text. Data represent arithmetic means ± SD for seven independent experiments (survival rate, $p = 0.225$; altered shape, $p < 0.001$). (B) Immunofluorescence analysis of NIH3T3 cells coexpressing *gas3/PMP22* and *AK* or *gas3/PMP22* and *rhoA*-V14 or *gas3/PMP22*. NIH3T3 cells 24 h after seeding were microinjected with pEXV-*gas3/PMP22FLAG* (100 ng/μl) and pEXV-*AK* (25 ng/μl) or with pEXV-*gas3/PMP22FLAG* (100 ng/μl) and pEXV-*RhoA-V14* (25 ng/μl). After 24 h cells were fixed and processed for immunofluorescence to visualize Gas3/PMP22FLAG. Bar, 5 μm.

Apoptosis and Morphological Changes Triggered by Gas3/PMP22 Are Differentially Counterbalanced by bcl-2 and RhoA

Previous experiments, in which Bcl-2 and gas3/PMP22 were coexpressed, suggested that although apoptosis was efficiently counteracted, cell shape and spreading changes were still detectable. In this context, Bcl-2 and RhoA could be useful tools to dissect the different biological activities of Gas3/PMP22. With this aim, we next decided to perform a quantitative analysis on the differential effects of RhoA and Bcl-2 on the Gas3/PMP22-induced phenotypes.

gas3/PMP22FLAG was coexpressed by nuclear microinjection in NIH3T3 cells together with *rhoA*-V14, *bcl-2*, or *AK* as a control gene. All the cDNAs were cloned in the same expression vector and microinjected, respectively, at the concentrations of 100 ng/μl (*gas3/PMP22FLAG*) and 25 ng/μl (*AK*, *bcl-2*, and *rhoA*-V14). Cells were grown for a further 24 h in 10% FCS and then scored both for Gas3/PMP22 expression and for morphological changes by immunofluorescence analysis.

As described above, coexpression of *bcl-2* increased the survival rate of cells expressing Gas3/PMP22 to 50.5 ± 14% compared with 26 ± 6.3% when *AK* was coexpressed ($p < 0.05$). Here again, *rhoA* only slightly increased cell survival, 33 ± 7.5% survival rate compared with 26 ± 6.3% (Figure 6A). An opposite result was obtained when we analyzed cell shape and spreading changes induced by *gas3/PMP22* overex-

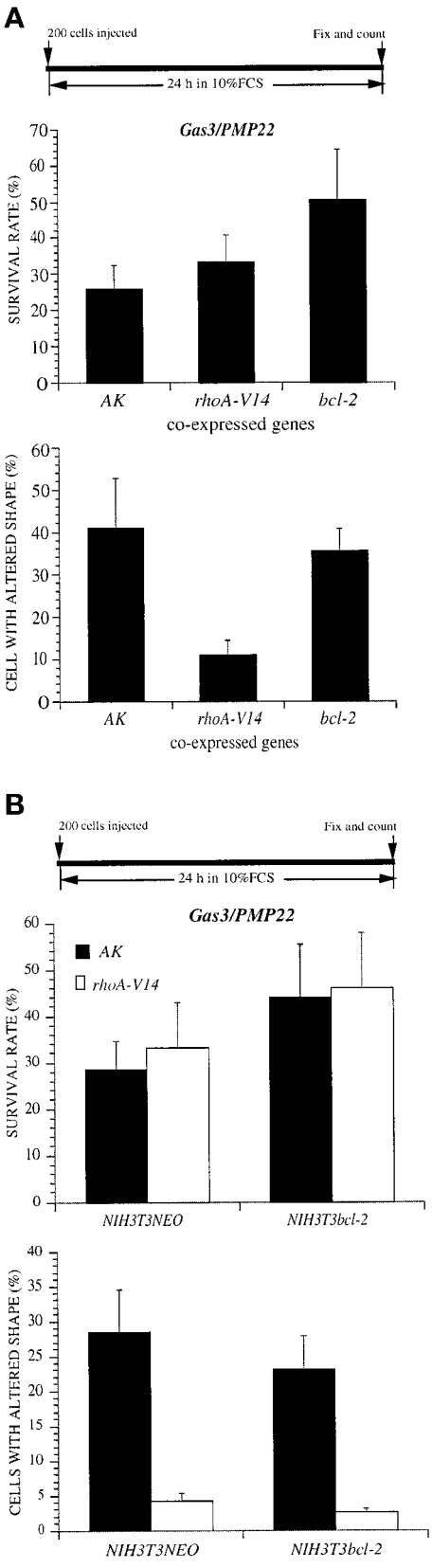

pression. Here again, RhoA-V14 efficiently counteracted Gas3/PMP22-dependent cell shape and spreading changes; 11 ± 3.3% of cells presented morphological alterations compared with the 41 ± 11.8% of the control ($p < 0.05$) (Figure 6A). On the contrary, coexpression of *bcl-2* only modestly interfered with the appearance of cell shape and spreading changes (35 ± 5.5% of the cells affected).

To further confirm the differential effect of Bcl-2 and RhoA-V14 on Gas3/PMP22-dependent changes in cell shape and survival, we decided to comicroinject *gas3/PMP22* with *rhoA-V14* or with *AK* in an NIH3T3 cell line stably expressing *bcl-2* (Brancolini *et al.*, 1995). As reported in Figure 6B, when *gas3/PMP22* was coexpressed with *rhoA-V14* in NIH3T3 *bcl-2* cells, survival was increased, and cell shape and spreading alterations were reduced. Therefore, the rescue of the phenotype induced by *gas3/PMP22* overexpression in NIH3T3 cells was possible only when both Bcl-2 and RhoA-V14 were simultaneously present.

Gas3/PMP22-dependent Changes in Cell Shape and Spreading Can Be Modulated by Bacterial Toxin-regulating Rho Activity

CNF1 from *Escherichia coli*, a toxin that activates Rho small GTPase, and the *Clostridium botulinum* C3 exotransferase, which inhibits Rho, have been widely used to study the role of this GTPase in different cellular processes (Fiorentini *et al.*, 1998). Therefore, they represent useful tools to confirm the role of this GTPase in regulating Gas3/PMP22 cell shape and spreading changes.

NIH3T3 cells were microinjected with 100 ng/μl pGDSV7*gas3/PMP22*-FLAG and grown for 24 in serum-free medium in the presence or absence of CNF1. In the control experiments >50 ± 7% of the Gas3/PMP22-overexpressing cells showed cell shape and spreading changes (Figure 7A). CNF1 treatment reduced to ~26 ± 6% the percentage of cells showing a Gas3/PMP22 phenotype, thus suggesting that endogenous Rho activity is sufficient to counteract the Gas3/PMP22-dependent effect on cell shape and spreading. Representative fields of cells expressing *gas3/*

Figure 6. Coexpression of Gas3/PMP22, RhoA-V14 and Bcl-2 in NIH3T3 cells. (A) *AK*, *rhoA*-V14, and *bcl-2* were coexpressed with *gas3/PMP22* in NIH3T3 cells. After 24 h from microinjection cells were fixed and processed for immunofluorescence to detect Gas3/PMP22FLAG. Survival and morphological changes were scored as described in the text. Data represent arithmetic means ± SD for seven independent experiments ($p < 0.001$). (B) *gas3/PMP22* and *rhoA-V14* were coexpressed in NIH3T3*NEO* and in NIH3T3*bcl-2* cells by nuclear microinjection. After 24 h from microinjection cells were fixed and processed for immunofluorescence to detect Gas3/PMP22FLAG. Survival and morphological changes were scored as described in the text. Data represent arithmetic means ± SD for three independent experiments.

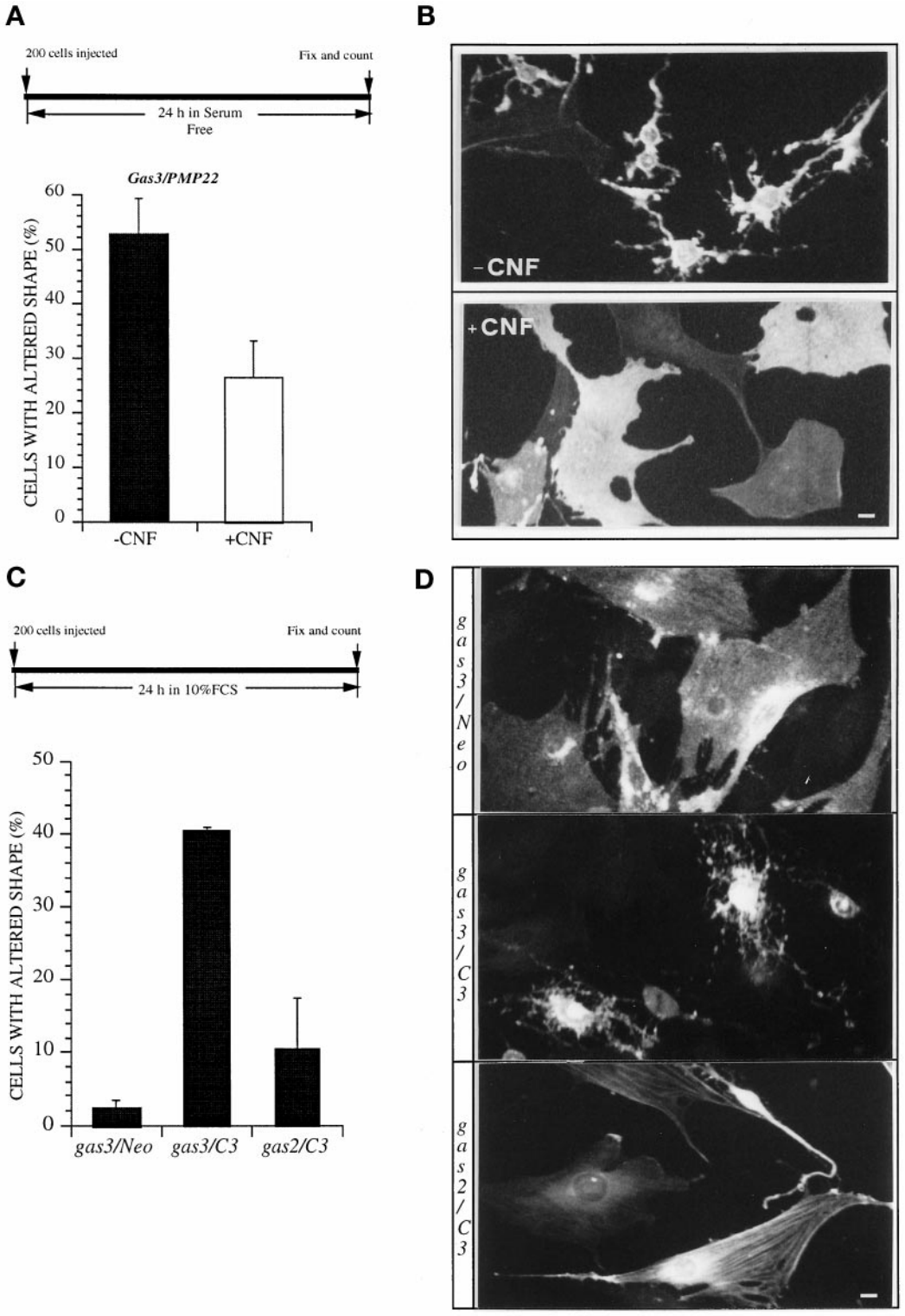

Figure 7. Gas3/PMP22 effect on cell shape and spreading can be modulated by bacterial toxin regulating Rho activity. (A) *gas3/PMP22* FLAG was overexpressed in NIH3T3 cells by nuclear microinjection. After microinjection cells were treated or not with CNF-1 in serum-free medium; 24 h later cells were fixed and processed for immunofluorescence to detect Gas3/PMP22FLAG. Morphological changes were scored as described in the text. Data represent arithmetic means ± SD for four independent experiments ($p = 0.002$). (B) Immunofluorescence

PMP22FLAG treated or not with CNF-1, as detected after immunofluorescence analysis, are reported in Figure 7B.

C3 exoenzyme is an ADP-ribosyltransferase that inhibits Rho by covalently linking ADP-ribose to Rho asparagine 48 (Fiorentini *et al.*, 1998). REF 52 cells are unresponsive to Gas3/PMP22 overexpression, thus representing the ideal system to confirm whether Rho is the critical player that mediates the Gas3/PMP22-dependent alterations in cell shape and spreading.

pGDSV7*gas3/PMP22FLAG* (100 ng/μl) was coexpressed by nuclear microinjection in REF 52 cells together with pcDNA*C3* (25 ng/μl) or pcDNA*NEO* (25 ng/μl). pGDSV7*gas2* (100 ng/μl) together with pcDNA*C3* (25 ng/μl) was used as control.

Overexpression of Gas3/PMP22 was unable to induce morphological changes in REF 52 cells, as previously described (Figure 7C). Coexpression of Gas2 with low amounts of C3 exoenzyme (25 ng/μl) induced morphological changes in ~10 ± 7% of the injected cells. However, when the same amount of C3 was coexpressed with Gas3/PMP22, REF 52 cells were made fully responsive, in terms of alterations of cell shape and spreading, to Gas3/PMP22 overexpression. In fact, after 24 h from microinjection ~40 ± 0.5% ($p < 0.05$) of the cells coexpressing Gas3/PMP22 and C3 cells showed a Gas3/PMP22 phenotype.

Representative fields of cells expressing *gas3/PMP22FLAG* and *Neo, gas3/PMP22FLAG* and *C3*, or *Gas2* and *C3*, as detected after immunofluorescence analysis, are reported in Figure 7D.

Overexpression of gas3/PMP22 CMT1A Point Mutations Shows a Significant Reduced Apoptotic Response and Was Unable to Trigger Morphological Changes

Different point mutations in the human gas3/PMP22 gene have been described in CMT1A patients (Patel and Lupski, 1994; Suter and Snipes, 1995). Therefore, we assessed whether the Gas3/PMP22 point mutants responsible for the CMT1A were able to modulate changes in cell shape and spreading.

We used the Gas3/PMP22 point mutants as found in human CMT1A (L16P and S79C) and one mutation carried by mice with the Trembler phenotype (G150D) (Fabbretti *et al.*, 1995). These mutations code for a single amino acid substitution within one of the four putative transmembrane domains of Gas3/PMP22.

gas3/PMP22FLAG and the different point mutations were overexpressed by nuclear microinjection in NIH3T3 cells. All the cDNAs were cloned in the same expression vector and microinjected at the concentration of 100 ng/μl. Cells were grown for further 24 h in 10% FCS and then scored both for Gas3/PMP22 expression and for morphological changes by immunofluorescence analysis.

Cell survival was appreciably increased in cells expressing the mutants, ~50% survival rate compared with the Gas3/PMP22 wild type (~30 ± 1% survival rate) (Figure 8), thus indicating that the apoptotic response was significantly reduced in the case of the Gas3/PMP22 point mutants as previously described (Fabbretti *et al.*, 1995).

An even more marked difference was observed for the number of cells showing altered shape. As shown in Figure 8, overexpression of the different Gas3/PMP22 point mutants analyzed was unable to trigger morphological changes.

Wortmannin Can Augment the Morphological Changes Induced by Gas3/PMP22 Overexpression in NIH3T3 Cells

Phosphatidylinositol lipids have been implicated in regulating the Rho family of small GTPases. Phosphoinositide 3-kinase (PI3K) might act upstream of the small GTPases in controlling cytoskeletal changes in response to extracellular factors (Kotani *et al.*, 1994; Wennstrom *et al.*, 1994; Van Aelst and D'Souza-Schorey, 1997).

To gain further insights on the mechanisms regulating the Gas3/PMP22-dependent morphological response, we analyzed whether two well-characterized PI3K inhibitors such as WT and LY294002 were able to agument such morphological response.

NIH3T3 cells were microinjected with 50 ng/μl pGDSV7*gas3/PMP22*-FLAG, and 6 h after microinjection they were treated with the different inhibitors. To discriminate a positive effect on the Gas3/PMP22-dependent modifications of cell shape and spreading, cells were fixed at an early time after microinjection (18 h).

After this period overexpression of Gas3/PMP22 induced cell shape and spreading alterations in ~17 ± 6% of injected cells (Figure 9A). WT treatment dramat-

Figure 7 (cont). analysis of NIH3T3 cells expressing *gas3/PMP22* in the presence of CNF-1. NIH3T3 cells 24 h after seeding were microinjected with pGDSV7-*gas3/PMP22FLAG* (100 ng/μl). After microinjection medium was changed to serum free, and cells were treated or not with CNF-1. Twenty-four hours later cells were fixed and processed for immunofluorescence to visualize Gas3/PMP22FLAG. Bar, 25 μm. (C) C3 exoenxyme was coexpressed with *gas3/PMP22* or *gas2* in REF 52 cells. After 24 h from microinjection cells were fixed and processed for immunofluorescence to detect Gas3/PMP22FLAG or Gas2. Morphological changes were scored as described in the text. Data represent arithmetic means ± SD for four independent experiments ($p < 0.001$). (D) Immunofluorescence analysis of REF 52 cells expressing *gas3/PMP22*. REF 52 cells 24 h after seeding were microinjected with pGDSV7-*gas3/PMP22FLAG* (100 ng/μl) and pcDNA3*NEO* (25 ng/μl), with pGDSV7-*gas3/PMP22FLAG* (100 ng/μl) and pcDNA3*C3* (25 ng/μl), or with pGDSV7-*gas2* (100 ng/μl) and pcDNA3*C3* (25 ng/μl). Twenty-four hours later cells were fixed and processed for immunofluorescence to visualize Gas3/PMP22FLAG or Gas2. Bar, 25 μm.

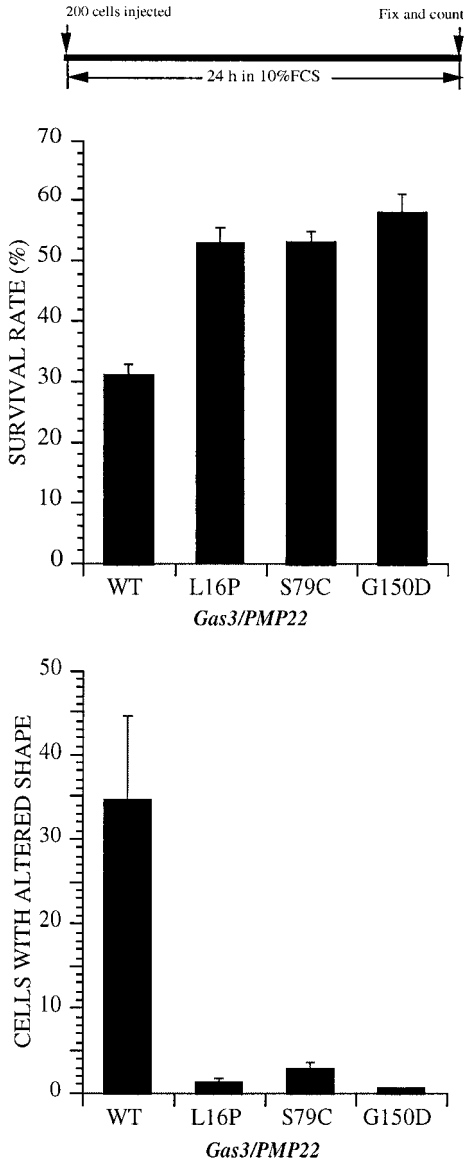

Figure 8. Overexpression of Gas3/PMP22 CMT1A point mutants in NIH3T3 cells. *gas3/PMP22*wt-FLAG, *gas3/PMP22*L16P-FLAG, *gas3/PMP22*S79C-FLAG, and *gas3/PMP22*G150D-FLAG were overexpressed in NIH3T3 cells by nuclear microinjection. After 24 h from microinjection cells were fixed and processed for immunofluorescence to detect Gas3/PMP22FLAG. Survival and morphological changes were scored as described in the text. Data represent arithmetic means ± SD for five independent experiments ($p < 0.001$).

ically increased the percentage (~44 ± 9%; $p < 0.05$), of Gas3/PMP22-overexpressing cells showing altered morphology (Figure 9, A and B). Under the same experimental conditions, LY294002 less efficiently raised the percentage of Gas3/PMP22-overexpressing cells showing altered morphology, reaching ~29 ± 5% of the injected cells ($p < 0.05$). The effect of Gas3/PMP22 on cell survival was unaffected after both WT and LY294002 treatments (Figure 9A). The reduced effect of LY294002 compared with WT could be dependent on a different half-life of inhibitors in our experimental system. In fact, when MAPK activation was assessed in our experimental system as marker of PI3K activity (Goruppi *et al*., 1997), WT was a more potent inhibitor than LY294002 (our unpublished results). In Figure 9B representative fields of cells expressing *gas3/PMP22FLAG* treated or not with WT, as detected after immunofluorescence analysis, are reported.

Having demonstrated a compelling effect of WT on Gas3/PMP22 morphological activity, we next analyzed whether RhoA-V14 was able to counteract such an effect.

gas3/PMP22FLAG was coexpressed in NIH3T3 cells together with *rhoA*-V14 or with *AK* as a control gene. Six hours after microinjection cells were treated with WT, and 12 h later they were fixed and processed for immnuofluorescence.

Under these experimental conditions coexpression of Gas3/PMP22 and of the control gene AK induced modification of cell shape and spreading in ~15 ± 3% of the injected cells (Figure 9C). Here again WT treatment dramatically increased, up to 35 ± 6% ($p < 0.05$), the percentage of Gas3/PMP22-overexpressing cells showing altered cell shape and spreading. On the contrary, in cells coexpressing Gas3/PMP22 and RhoA-V14, WT treatment was unable to exhibit any clear effect on cell morphology (Figure 9C).

The effect of Gas3/PMP22 on cell survival was unaffected by WT treatment.

Gas3/PMP22 Overexpression Can Interfere with LPA-dependent Stress Fiber Formation

Having demonstrated an interference of RhoA on Gas3/PMP22-dependent changes of cell shape and spreading, we next attempted to understand whether Gas3/PMP33 could interfere with a Rho activity

Lysophosphatidic acid (LPA) stimulates, in a Rho-dependent manner, the assembly of stress fibers and the formation of focal adhesion complexes in fibroblasts (Ridley and Hall, 1992; Machesky and Hall, 1996). Therefore, we analyzed the response to LPA, in terms of stress fibers formation, in cells overexpressing Gas3/PMP22.

Stress fibers extending throughout the cell body can be induced in quiescent, serum-starved Swiss 3T3 cells by addition of LPA (Figure 10, A and B). In cells overexpressing Gas3/PMP22 and showing the above-described morphological changes, the assembly of stress fibers was impaired. In a typical cell overexpressing Gas3/PMP22 (Figure 10, C and D, arrow), stress fibers were barely detectable; instead actin staining can be observed as punctuate pattern throughout the cell. An alteration in stress fiber formation in re-

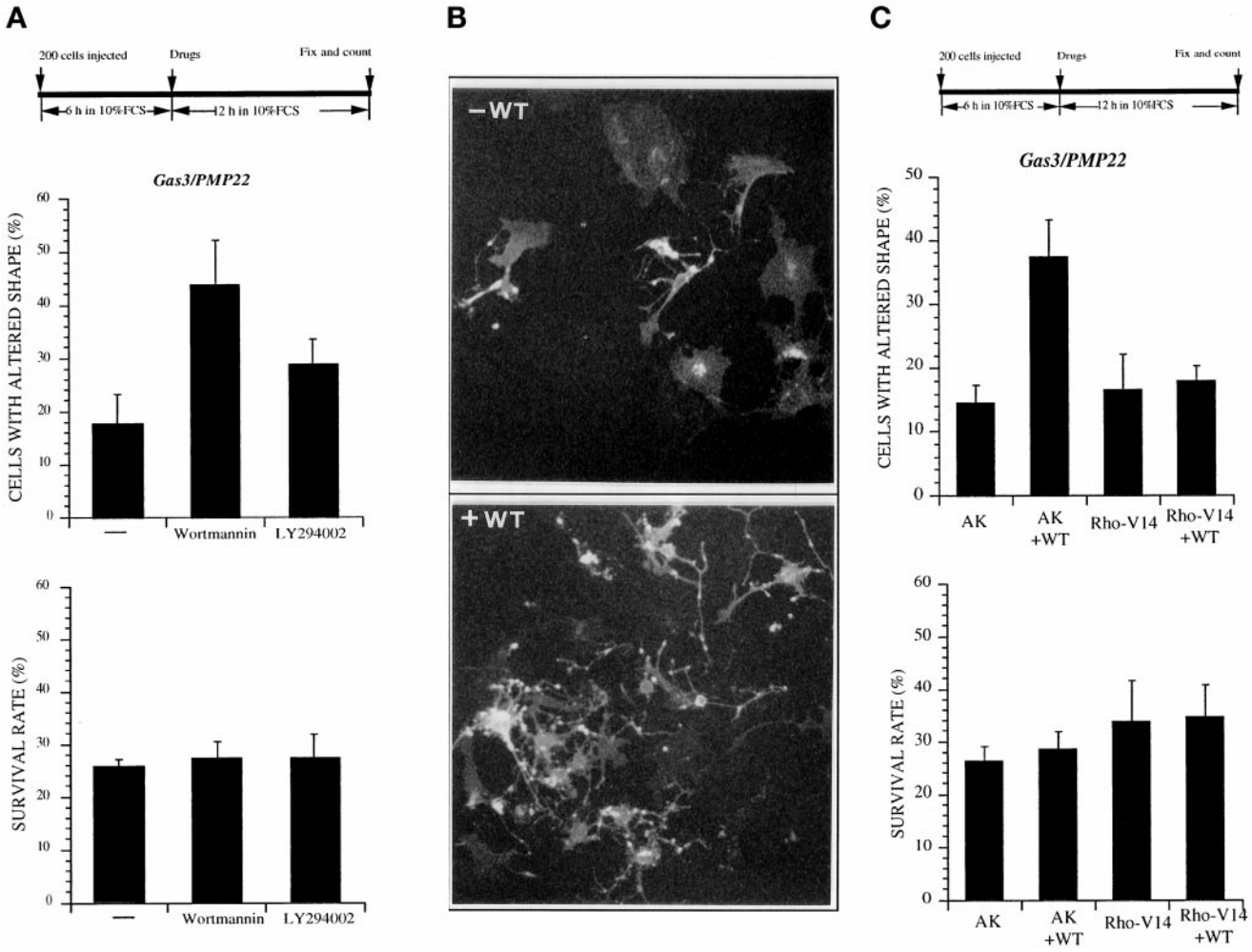

Figure 9. Wortmannin (WT) can agument changes of cell shape and spreading induced by Gas3/PMP22. (A) *gas3/PMP22* FLAG was overexpressed in NIH3T3 cells by nuclear microinjection. After 6 h cells were treated or not with WT and LY294002; 12 h later cells were fixed and processed for immunofluorescence to detect Gas3/PMP22FLAG. Survival and morphological changes were scored as described in the text. Data represent arithmetic means ± SD for five independent experiments (altered shape, $p < 0.001$). (B) Immunofluorescence analysis of NIH3T3 cells expressing *gas3/PMP22* in the presence of WT. NIH3T3 cells 24 h after seeding were microinjected with pEXV-*gas3/PMP22FLAG* (50 ng/μl). After 6 h cells were treated or not with WT; 12 h later cells were fixed and processed for immunofluorescence to visualize Gas3/PMP22FLAG. Bar, 25 μm. (C) *AK* and *rhoA*-V14 were coexpressed with *gas3/PMP22* in NIH3T3 cells. After 6 h cells were treated or not with WT; 12 h later cells were fixed and processed for immunofluorescence to detect Gas3/PMP22FLAG. Survival and morphological changes were scored as described in the text. Data represent arithmetic means ± SD for five independent experiments (altered shape, $p < 0.001$).

sponse to LPA was also observed in cells overexpressing lower levels of Gas3/PMP22; therefore, the cells do not showing dramatic signs of shape and spreading changes. A representative cell is shown in Figure 9, E and F; here few stress fibers were observed in response to LPA, and they rarely traversed the cell body; on the contrary, patches of actin filaments were present (Figure 10, E and F, arrowheads).

To visualize focal adhesion complexes, Gas3/PMP22-overexpressing and LPA-treated cells were immunofluorescently stained for the focal adhesion protein talin. As shown in Figure 10, G and H (arrowheads), also focal adhesion complex assembly in response to LPA was reduced in cells overexpressing Gas3/PMP22 compared with the uninjected cells.

In summary, the Rho-dependent changes of the microfilament system in response to LPA were impaired in Gas3/PMP22-overexpressing cells.

DISCUSSION

Different elegant in vivo studies on Gas3/PMP22 have been fundamental in confirming the crucial role of this protein in regulating myelin formation and stability and its involvement in different human peripheral neuropathies (Adlkofer *et al.*, 1995, Hux-

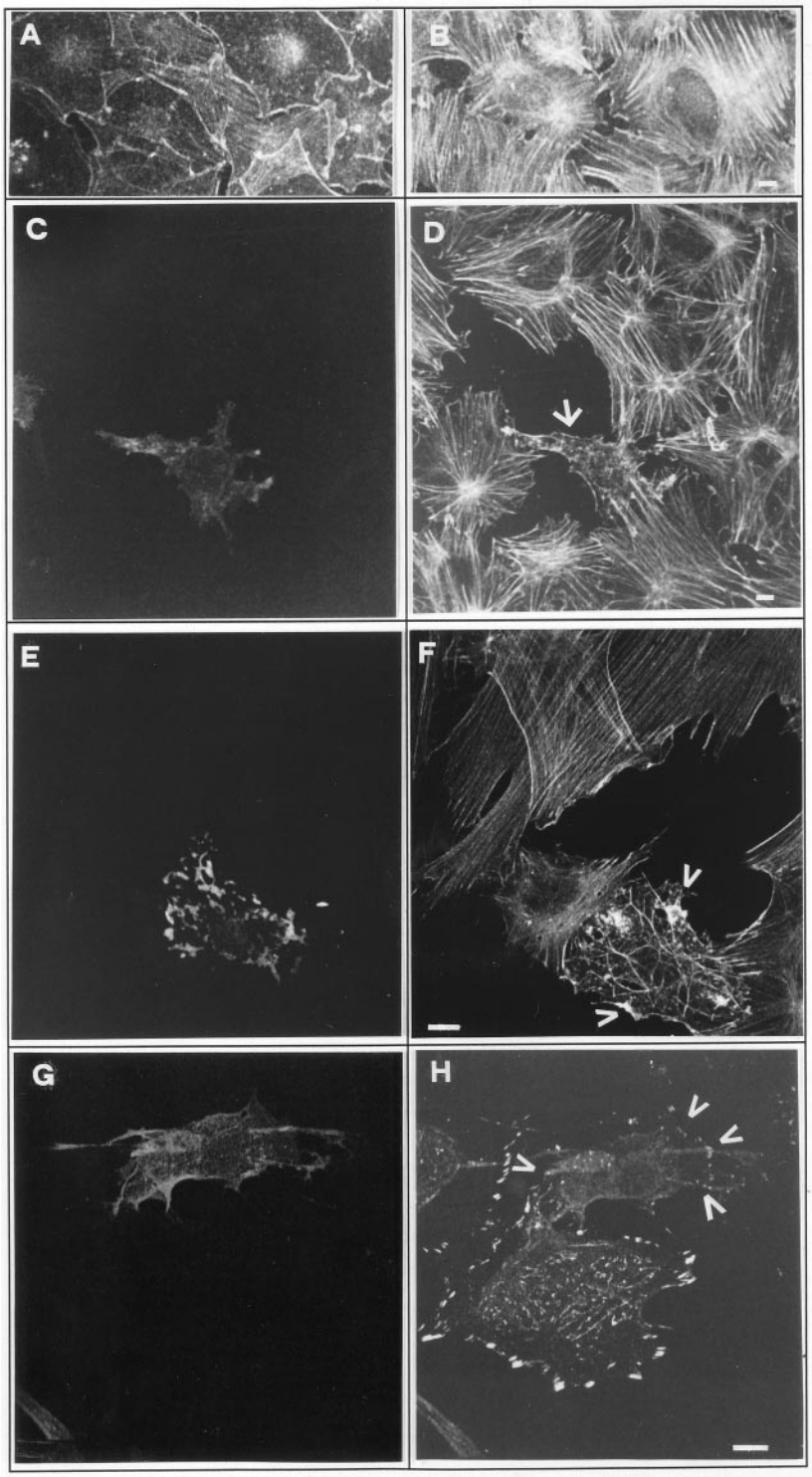

Figure 10. Gas3/PMP22 overexpression and stress fiber formation. Swiss 3T3 grown for 48 h in 0.1% FCS (A) and then treated for 30 min with LPA (B) were stained to visualize microfilaments. Serum-starved Swiss 3T3 cells were microinjected with pEXV*hGas3/PMP22* (100 ng/μl). After 15 h from microinjection, LPA was added, and 30 min later cells were fixed and processed for immunofluorescence analysis to visualize actin filaments (D and F), Gas3/PMP22 (C, E, and G) and talin (H). Arrows indicate microinjected cells. Bar, 10 μm.

ley *et al*., 1996; Magyar *et al*., 1996; Sereda *et al*., 1996, D'Urso *et al*., 1997). On the other hand, they have been unable to unveil the biological mechanisms regulated by Gas3/PMP22. Furthermore, the discovery of Gas3/PMP22-related proteins also expressed in myelinating Schwann cells (Kaprielian *et al*., 1995; Schaeren-Wiemers *et al*., 1995; Gillen *et al*., 1996; Taylor and Suter, 1996; Bolin *et al*., 1997) adds

additional complexity to the problem of the in vivo studies, in which compensatory mechanisms might also exist. In this regard, our strategy, based on a transient overexpression in cultured cells, could represent a useful approach to define the functional roles of Gas3/PMP22.

In this report we have unveiled a role of *gas3/PMP22* in regulating cell morphology, as evidenced in terms of reduced cell spreading, which can be separated from the previously reported apoptotic response.

The Gas3/PMP22-dependent morphological response was easily detectable when the apoptotic response was counteracted by antiapoptotic genes such as *bcl-2* and *crmA*. In our experiments Bcl-2 was consistently more efficient in counteracting apoptosis triggered by Gas3/PMP22 with respect to CrmA. Bcl-2 (Reed, 1997; Green and Kroemer, 1998; Silke and Vaux, 1998) is a broad inhibitor of caspases, a family of cysteine-protease, which plays a critical role in the execution of the apoptotic program (for review, see Cohen, 1997; Crynes and Yuan, 1998), whereas CrmA, a 38-kDa serpin from cowpox virus, is a potent inhibitor of some caspases, such as caspase-1 and 8, but a weak inhibitor for others such as caspase-3 and -2 (Ray e*t al.*, 1992; Nicholson *et al.*, 1995; Sirinivasula *et al.*, 1996; Cohen, 1997). Therefore, the relative pattern of caspase inhibition reflects the differential effect of Bcl-2 and CrmA on Gas3/PMP22 apoptotic response. In addition, these data indicate that Gas3/PMP22 can trigger a "classical" apoptotic response, characterized by caspase activation.

The time-lapse analysis confirmed that overexpression of *gas3/PMP22* induces, precedent or parallel to the apoptotic response, morphological changes that can be observed as a reduction in cell spreading.

This phenotype was specific for Gas3/PMP22 because overexpression of P_0, another component of compact myelin, was unable to induce changes in cell spreading. Moreover, the gas3/PMP22 point mutations associated with CMT1A and Trembler failed to induce changes in cell spreading when similarly overexpressed in NIH3T3 cells. This evidence indicates that the effect of Gas3/PMP22 on cell spreading is strictly linked to the disease and therefore to the process of myelinization in vivo.

The effect of Gas3/PMP22 on cell morphology and spreading involved the small GTPase Rho (for review, see Machesky and Hall, 1996; Van Aelst and D'Souza-Schorey, 1997; Hall, 1998). Different pieces of evidence support this conclusion: 1) coexpression of an active form of RhoA can efficiently counteract the morphological changes induced by Gas3/PMP22; 2) the bacterial toxin CNF1 from *E. coli,* which activates Rho, can also counteract the Gas3/PMP22 phenotype; and 3) the *C. botulinum* exoenzymes C3, which inhibits Rho activity, can transform the REF 52 cells, normally refractory to Gas3/PMP22 overexpression in a highly responsive cell line.

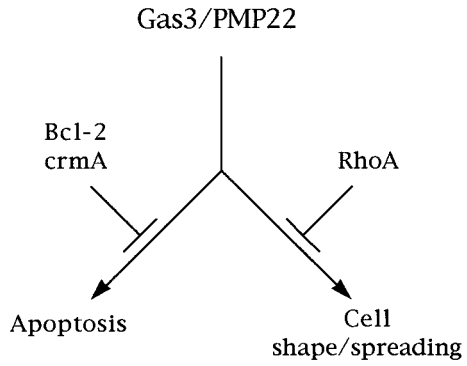

Figure 11. Schematic representation of Gas3/PMP22 biological activities. Gas3/PMP22 could regulate both susceptibility to apoptosis and morphological changes. Bcl-2 counteracts the apoptotic response, whereas Rho specifically counteracts morphological changes.

Our results obtained with the bacterial toxins, and in particular the recovery of a Gas3/PMP22 response in REF 52 cells when endogenous Rho was inhibited by C3 exoenzyme, strongly support the idea that the endogenous Rho is the critical switch to regulate cell shape and spreading changes in response to Gas3/PMP22.

Interestingly if an active Rho specifically suppressed the morphological response triggered by Gas3/PMP22, it was unable to efficiently counteract Gas3/PMP22-dependent apoptosis. Conversely, Bcl-2 specifically interfered with the apoptotic response, but it was unable to interfere with the morphological response. This clearly indicates that apoptosis and cell shape and spreading changes represent two distinct responses primed by Gas3/PMP22, thus suggesting that such signal should be branching at some point (Figure 11).

Rho GTPase is required for many actin-dependent cellular processes, such as platelet aggregation, lymphocyte and fibroblast adhesion, cell motility, contraction, and cytokinesis (Ridley and Hall, 1992; Narumiya *et al.*, 1997; Hall, 1998). Several direct targets of Rho have been identified (for review, see Van Aelst and D'Souza-Schorey, 1997). Among them the Rho-associated kinases seem to mediate RhoA effects on actin cytoskeleton (Leung *et al.*, 1995; Ishizaki *et al.*, 1996; Amano *et al.*, 1997). These kinases can regulate cell contractility by directly phosphorylating myosin light chain or indirectly by phosphorylating and inhibiting myosin light chain phosphatase (Amano *et al.*, 1996; Kimura *et al.*, 1996). More recently also members of the ezrin/radixin/moesin family of proteins, which are required to mediate the Rho-dependent stress fiber

assembly and focal complex formation (Mackay *et al.*, 1997), seem to be modulated by Rho kinases (Matsui *et al.*, 1998). Regulation of phosphatidylinositol-4,5-biphosphate synthesis is another key event orchestrating the actin cytoskeleton, but it is still unclear whether phosphatidylinositol 4-phosphate 5-kinase interacts with Rho directly (Van Aelst and D'Souza-Schorey, 1997; Hall, 1998). Within this complex scenario it would be of great interest to determine which Rho-specific target is necessary to modulate Gas3/PMP22 activity on cell shape and spreading.

The Gas3/PMP22 dependent alteration of cell shape and spreading was dramatically increased by WT and to a lesser extent by LY294002, thus possibly suggesting an involvement of a PI3K in antagonizing such activity. WT and LY294002 are commonly used as inhibitors of PI3K; however, at micromolar concentrations they can also inhibit a phosphatidylinositol 4-kinase (Nakanishi *et al.*, 1995; Carpenter and Cantley, 1996); therefore, further studies will be necessary to confirm an involvement of PI3K in regulating Gas3/PMP22 morphological signaling. Nevertheless, it is interesting to note that Cdc42, Rac, and Rho can operate in a hierarchical cascade wherein CDC42 activates Rac, which in turn activates Rho (Nobes and Hall, 1995). Experiments using WT suggest that PI3K might act upstream of Rac (Kotani *et al.*, 1994; Wennstrom *et al.*, 1994; Nobes *et al.*, 1995; Van Aelst and D'Souza-Schorey, 1997), and a constitutively active PI3K kinase mutant was able to trigger membrane ruffles and stress fibers in a Rac- and Rho-dependent manner (Reif *et al.*, 1996). We noticed that the WT reinforcement of the Gas3/PMP22 phenotype was efficiently suppressed by an active RhoA. Therefore, it is possible that the effect of WT on Gas3/PMP22-triggered morphological changes could be dependent on the PI3K-regulated Rho activity.

How could the effect of Gas3/PMP22 on cell shape and spreading, possibly by acting on Rho GTPase, contribute to myelin formation and stability? Studies made in melanocytes, astrocytes, and neuronal cells have shown that changes in microfilament organization and cell shape, such as dendrite and neurite outgrowth, which are linked to a differentiative response, require Rho inhibition (Gebbink *et al.*, 1997; Jin and Strittmatter, 1997; Busca *et al.*, 1998; Ramakers and Moolenaar, 1998). Altogether these reports support a model in which inactivation of Rho is the necessary requirement to promote specific cytoskeletal and morphological changes characterizing the differentiated phenotype. In this regard we can speculate that changes in cell shape and actin architecture occurring during differentiation of the Schwann cells, which lead to myelinization, require Rho inhibition. In this scenario there are two possible explanations for the observed functional link between Gas3/PMP22 and Rho. Gas3/PMP22-dependent regulation of cell shape and spreading could only be possible after Rho inactivation, which might occur independently of Gas3/PMP22. Alternatively, Gas3/PMP22 might regulate Rho signaling within the cells, thus leading to changes in cell shape and spreading necessary for myelinization. We favor the second possibility, and some evidence supports our speculation. Gas3/PMP22 can interfere with the LPA-triggered assembly of stress fibers and focal adhesion complexes. LPA-mediated activation of Rho and attachment of integrins to the extracellular matrix are both required for cell spreading and formation of focal complexes, whereas Rho-dependent assembly of stress fibers is not dependent from extracellular matrix (Hotchin *and* Hall, 1995). Because in cells overexpressing Gas3/PMP22 stress fiber assembly in response to LPA was impaired, it is therefore possible that Gas3/PMP22 regulates, in a still undefined manner, Rho activity within the cell. In addition, it is important to note that at early stages of myelinogenesis, PMP22-deficient peripheral nerves are retarded in myelin formation, and it has been suggested that Gas3/PMP22 could be a component of the complex mechanism contributing to the driving force for turning the Schwann cell loops around the axon (Adlkofer *et al.*, 1995).

Gas3/PMP22 should also be involved in regulating myelin thickness and stability, because PMP22-deficient mice show redundant myelin loops with normal spacing (tomacula), together with signs of myelin degeneration at a more advanced stage (Adlkofer *et al.*, 1995). Indeed, a specific organization of the actin cytoskeleton associated with the myelin envelope has been proposed based on localization studies of the actin capping and severing protein gelsolin (Tanaka and Sobue, 1994).

In conclusion, we have demonstrated that two different biological functions can be ascribed to Gas3/PMP22, and we have explored the correlation between a tetraspan protein and the small GTPase Rho. How this relates to the differentiation and myelinization of the Schwann cells and to the peripheral neuropathies is an intriguing question that can now be investigated.

ACKNOWLEDGMENTS

We are grateful to Alan Hall (Medical Research Council Laboratory University College, London, United Kingdom) for the pEXV-rhoAV14 construct, Craig B. Thompson (University of Chicago, Chicago, IL) for bax cDNA, Licio Collavin (Laboratorio Nazionale Consorzio Interuniversitario Biotecnologie) for AK cDNA, Ding Xue (Massachusetts Institute of Technology, Boston, MA) for crmA cDNA, and Donatella D'Urso (University of Dusseldorf, Dusseldorf, Germany) for P_0 cDNA. We thank Guido Tarone (University of Torino, Torino, Italy) for fibronectin and useful

comments and Juan J. Archelos (University of Wurzburg, Wurzburg, Germany) for anti-P_0 monoclonal antibody. We are indebted to Lawrence Wrabetz (Department of Biological and Technological Research, Milan, Italy) for very useful comments and suggestions on the manuscript. This work was supported by Telethon-Progetto grant 770 (to C.S.).

REFERENCES

Adlkofer K., Martini, R., Aguzzi, A., Zielasek, J., Toyka K.V., and Suter, U. (1995). Hypermyelination and demyelinating peripheral neuropathy in PMP22-deficient mice. Nat. Genet. *11*, 274–280.

Amano, M., Chiahara, K., Kimura, K., Fukuta, Y., Nakamura, N., Matsuura, Y., and Kaibuchi, K. (1997). Formation of actin stress fibers and focal adhesions is enhanced by Rho kinase. Science *275*, 1308–1311.

Amano, M., Ito, M., Kimura, K., Fukata, Y., Chihara, K., Nakano, T., Matsuura, Y., and Kaibuchi, K. (1996). Phosphorylation and activation of myosin by Rho-associated kinase (Rho-kinase). J. Biol. Chem. *271*, 20246–20249.

Archelos, J.J., Roggenbuck, K., Schneider-Schaulies, J., Linington, C., Toyka K.V., and Hartung, H.P. (1993). Production and characterization of monoclonal antibodies to the extracellular domain of P0. J. Neurosci. Res. *35*, 46–53.

Baechner, D., Liehr, T., Hameister, H., Altenberger, H., Grehl, H., Suter, U., and Rautenstrauss, B. (1995). Widespread expression of the peripheral myelin protein-22 gene (pmp22) in neural and non-neural tissue during murine development. J. Neurosci. Res. *42*, 733–741.

Bolin, L.M., McNeil, T., Lucian, L.A., DeVaux, B., Franz-Bacon, K., Gorman, D.M., Zurawski, S., Murray, R., and McClanahan, T.K. (1997). HNMP-1: a novel hematopoietic and neural membrane protein differentially regulated in neural development and injury. J. Neurosci. *17*, 5493–5502.

Brancolini, C., Benedetti, M., and Schneider, C. (1995). Microfilament reorganization during apoptosis: the role of Gas2, a possible substrate for ICE-like proteases. EMBO J. *14*, 5179–5190.

Brancolini, C., Marzinotto, S., and Schneider, C. (1997). Susceptibility to p53 dependent apoptosis correlates with increased levels of Gas2 and Gas3 proteins. Cell Death Differ. *4*, 247–253.

Brockes, J.P., Fields, K.L., and Raff, M.C. (1979). Studies on cultured rat Schwann cells I. Establishment of purified populations from cultures of peripheral nerve. Brain Res. *165*, 105–118.

Busca, R., Bertolotto, C., Abbe, P., Englaro, W., Ishizaki, T., Narumiya, S., Boquet, P., Ortonne, J.-P., and Ballotti, R. (1998). Inhibition of Rho is required for cAMP-induced melanoma cell differentiation. Mol. Biol. Cell *9*, 1367–1378.

Carpenter, C.L., and Cantley, L.C. (1996). Phosphoinositide kinase. Curr. Opin. Cell. Biol. *8*, 153–158.

Chance, P.F., Alderson, M.K., Leppig, K.A., Lensch, M.W., Matsunami, N., Smith, B., Swanson, P.D., Odelberg, S.J., Disteche, C.M., and Bird, T.D. (1993). DNA deletion associated with hereditary neuropathy with liability to pressure palsies. Cell *72*, 143–151.

Cohen, G.M. (1997). Caspases: the executionerof apoptosis. Biochem. J. *326*, 1–16.

Crynes, V., and Yuan, J. (1998). Proteases to die for. Genes & Dev. *12*, 1551–1570.

D'Urso, D., Schmalenbach, C., Zoidl, G., Prior, R., and Muller, H.W. (1997). Studies on the effect of altered PMP22 expression during myelination in vitro. J. Nerosci. Res. *48*, 31–42.

Edomi, P., Martinotti, A., Colombo, M.P., and Schneider, C. (1993). Sequence of human *gas3/PMP22* full-length cDNA. Gene *126*, 289–290.

Fabbretti, E., Edomi, P., Brancolini, C., and Schneider, C. (1995). Apoptotic phenotype induced by overexpression of the wilde type gas3/PMP22: its relation to the demyelinating peripheral neuropathy CMT1A. Genes & Dev. *9*, 1846–1856.

Fiorentini, C., Fabbri, A., Flatau, G., Donelli, G., Matarrese, P., Lemichez, E., Falzano, L., and Boquet, P. (1997). *Escherichia coli* cytotoxic necrotizing factor 1 (CNF1), a Toxin that activates the Rho GTPase. J. Biol. Chem. *272*, 19532–19537.

Fiorentini, C., Gauthier, M., Donelli, G., and Bouquet, P. (1998). Bacterial toxins and the Rho GTP-binding protein:what microbes teach us about cell regulation. Cell Death Differ. *5*, 720–728.

Gebbink, M., Kranenburg, O., Poland, M., van Horck, F., Houssa, B., and Moolenaar, W.H. (1997). Identification of a novel putative Rho-specific GDP/GTP exchange factor and a RhoA-binding protein: control of neuronal morphology. J. Cell Biol. *137*, 1603–1613.

Gillen, C., Gleichmann, M., Greiner-Petter, R., Zoidl, G., Kupfer, S., Bosse, F., Auer, J., and Muller, H.W. (1996). Full-length cloning, expression and cellular localization of rat plasmolipin mRNA a proteolipid of PNS and CNS. Eur. J. Neurosci. *8*, 405–414.

Goruppi, S., Ruaro, E., Varnum, B., and Schneider, C. (1997). Requirement of phosphotidylinositol 3-kinase-dependent pathway and src for Gas6-Axl mitogenic and survival activities in NIH3T3 fibroblasts. Mol. Cell. Biol. *17*, 4442–4453.

Green, D., and Kroemer, G. (1998). The central executioners of apoptosis: caspases or mitochondria? Trends Cell Biol. *8*, 267–271.

Hall, A. (1998). Rho GTPases and the actin cytoskeleton. Science *279*, 509–514.

Hotchin, N.A., and Hall, A. (1995). The assembly of integrin adhesion complexes requires both extracellular matrix and intracellular rho/rac GTPase. J. Cell Biol. *131*, 1857–1865.

Huxley, C., Passage, E., Manson, A., Putzu, G., Figarella-Branger, D., Pellissier, J.F., and Fontes, M. (1996). Construction of a mouse model of Charcot-Marie-Tooth disease type 1A by pronuclear injection of human YAC DNA. Hum. Mol. Genet. *5*, 563–569.

Ishizaki, T., *et al*. (1996). The small GTP-binding protein Rho binds to and activates a 160 kDa Ser/Th protein kinase homologus to myotonic dystrophy kinase. EMBO J. *15*, 1885–1893.

Jin, Z., and Strittmatter, S.M. (1997). Rac-1 mediates collapsin-1-induced growth cone collapse. J. Neurosci. *17*, 6256–6263.

Kaprielian, Z., Cho, K.O., Hadjiargyrou, M., and Patterson, P.H. (1995). CD9, a major platelet cell surface glycoprotein, is a ROCA antigen and is expressed in the nervous system. J. Neurosci. *15*, 574–583.

Kimura, K., *et al*. (1996). Regulation of myosin phosphatase by Rho and Rho-associated kinase (Rho-kinase). Science *273*, 245–248.

Kotani, K., *et al*. (1994). Involvement of phosphoinositide 3-kinase in insulin- or IGF-1-induced membrane ruffling. EMBO J. *13*, 2313–2321.

Leung, T., Manser, E., Tan, L., and Lim, L. (1995). A novel serine/threonine kinase binding the ras-related RhoA GTPase which translocates to the peripheral membranes. J. Biol. Chem. *270*, 29051–29054.

Lemke, G., Lamar, E., and Patterson, J. (1988). Isolation and analysis of the gene encoding peripheral myelin myelin protein zero. Cell *40*, 501–508.

Lupski, J.R., *et al*. (1991). DNA duplication associated with Charcot-Marie-Tooth disease type 1A. Cell *66*, 219–232.

Machesky, L.M., and Hall, A. (1996). Rho: a connection between membrane receptor signaling and the cytoskeleton. Trends Cell Biol. *6*, 304–310.

Mackay, D.J.G., Esch, F., Furthmayr, H., and Hall, A. (1997). Rho- and Rac-dependent assembly of focal adhesion complexes and actin filaments in permeabilized fibroblasts: an essential role for ezrin/radixin/moesin proteins. J. Cell Biol. *138*, 927–938.

Magyar, J.P., Ebensperger, N., Schaeren-Wiemers, N., and Suter, U. (1997). Myelin and lymphocyte protein (MAL/MVP17/VP17) and plasmolipin are members of an extended gene family. Gene *189*, 269–275.

Magyar, J.P., Martini, R., Ruelicke, T., Aguzzi, A., Adlkofer, K., Dembic, Z., Zielasek, J., Toyka, K.V., and Suter, U. (1996). Impaired differentiation of Schwann cells in transgenic mice with increased PMP22 gene dosage. J. Neurosci. *16*, 5351–53060.

Manfioletti, G., Ruaro, M.E., Del Sal, G., Philipson, L., and Schneider, C. (1990). A growth arrest-specific (gas) gene codes for a membrane protein. Mol. Cell. Biol. *10*, 2924–2930.

Marvin, K.W., Fujimoto, W., and Jetten, A.M. (1995). Identification and characterization of a novel squamous cell-associated gene related to PMP22. J. Biol. Chem. *270*, 28910–28916.

Matsui, T., Maeda, M., Dori, Y., Yonemura, S., Amano, M., Kaibuchi, K., Tsukita, S., and Tsukita, S. (1998). Rho-kinase phosphorylates COOH-terminal threonines of ezrin/radixin/moesin (ERM) proteins and regulates their head-to tail association. J. Cell Biol. *140*, 647–657.

Matsunami, N., *et al*. (1992). Peripheral myelin protein-22 gene maps in the duplication in chromosome 17p11.2 associated with Charcot-Marie-Tooth type 1A. Nat. Genet. *1*, 176–179.

McCarthy, N.J., Whyte, M.K.B., Gilber, C.S., and Evan, G.I. (1997). Inhibition of ced-3/ICE related proteases does not prevent cell death induced by oncogenes, DNA damage, or the Bcl-2 hommologue Bak. J. Cell Biol. *136*, 215–227.

Nakanishi, S., Catt, K.J., and Balla, T. (1995). A wortmannin-sensitive phosphatidylinositol 4-kinase that regulates hormone-sensitive pools of inositolphospholipids. Proc. Natl. Acad. Sci. USA *92*, 5317–5321.

Narumiya, S., Ishizaki, T., and Watanabe, N. (1997). Rho effectors and reorganization of actin cytoskeleton. FEBS Lett. *410*, 68–72.

Nicholson, D.W., *et al*. (1995). Identification and inhibition of the ICE/CED3 protease necessary for mammalian apoptosis. Nature *376*, 37–43.

Nobes, C.D., and Hall, A. (1995). Rho, rac, cdc42 GTPase regulate the assembly of multimolecular focal complexes associated with actin stress fiber, lamellipodia, and filopodia. Cell *81*, 53–62.

Nobes, C.D., Hawkins, P., Stephens, L., and Hall, A. (1995). Activation of the small GTP-binding proteins rho and rac by growth factor receptors. J. Cell Sci. *108*, 225–233.

Oltvai, Z.N., Milliman, C.L., and Korsmeyer, S.J. (1993). Bcl-2 heterdimerizes in vivo with a conserved homolog, Bax, that accelerates programmed cell death. Cell *74*, 609–619.

Patel, I.P., and Lupski, J.R. (1994). Charcot-Marie-Tooth disease: a new paradigm for the mechanism of inherited disease. Trends Genet. *10*, 128–133.

Patel, I.P., *et al*. (1992). The gene for the peripheral myelin protein PMP-22 is a candidate for Charcot-Marie-Tooth disease type 1A. Nat. Genet. *1*, 159–165.

Ramakers, G.J.A., and Moolenaar, W.H. (1998). Regulation of astrocyte morphology by RhoA and lysophosphatidic acid. Exp. Cell Res. *245*, 252–262.

Ray, C.A., Black, R.A., Kronheim, S.R., Greenstreet, T.A., Sleath, P.R., Salvesen, G.S., and Pickup, D.J. (1992). Viral inhibition of inflammation: cowpox virus encodes an inhibitor of the interleukin-1β converting enzyme. Cell *69*, 597–604.

Reed, J.C. (1997). Double identity for proteins of the Bcl-2 family. Nature *387*, 773–776.

Reif, K., Nobes, C.D., Thomas, G., Hall, A., and Cantrell, D.A. (1996). Phosphatidylinositol 3-kinase signals activates a selective subset of Rac/Rho effector pathways. Curr. Biol. *6*, 1445–1455.

Ridley, A.J., and Hall, A. (1992). The small GTP-binding protein rho regulates the assembly of focal adhesions and actin stress fibers in response to growth factors. Cell *70*, 389–399.

Ridley, A.J., Paterson, H.F., Johnston, C.L., Diekmann, D., and Hall, A. (1992). The small GTP-binding protein rac regulates growth factor-induced membrane ruffling. Cell *70*, 401–410.

Roa, B.B., Dyck, P.J., Marks, H.G., Chance, P.F., and Lupski, J.R. (1993a). Dejerine-Sottas syndrome associated with point mutation in the peripheral myelin protein 22 (PMP22) gene. Nat. Genet. *5*, 269–273.

Roa, B.B., Garcia, C.A., Suter, U., Kulpa, D.A., Wise, C.A., Müller, J., Welcher, A.A., Snipes, G.J., Shooter, E.M., and Patel, P. (1993b). Charcot-Marie-Tooth disease type 1A. Association with a spontaneous point mutation in the PMP22 gene. N. Engl. J. Med. *329*, 96–101.

Schaeren-Wiemers, N., Valenzuela, D.M., Frank, M., and Schwab, M.E. (1995). Characterization of the rat gene, rMAL, encoding a protein with four hydrophobic domains in central and peripheral myelin. J. Neurosci. *15*, 5753–5764.

Sereda, M., *et al*. (1996). A transgenic rat model of Charcot-Marie-Tooth disease. Neuron *16*, 1049–1060.

Silke, J., and Vaux, D.L. (1998). Cell death: shadow baxing. Curr. Biol. *8*, 528–531.

Sirinivasula, S.M., Ahmad, M., Fernandes-Alnemri, T., Litwack, G., and Alnemri, E.S. (1996). Molecular ordering of the Fas-apoptotic pathway: the Fas/APO-1 protease Mch5 is a crmA-inhibitable protease that activates multiple ced-3/ICE-like cystein proteases. Proc. Natl. Acad. Sci. USA *93*, 14486–14491.

Snipes, G.J., Suter, U., Welcher, A.A., and Shooter, E.M. (1992). Characterization of a novel peripheral nervous system myelin protein (PMP22/SR13). J. Cell Biol. *117*, 225–238.

Spreyer, P., Kuhn, G., Hanemann, C.O., Gillen, C., Schaal, H., Kuhn, R., Lemke, G., and Müller, H.W. (1991). Axon-regulated expression of a Schwann cell transcript that is homologous to a "growth arrest-specific" gene. EMBO J. *10*, 3661–3668.

Suter, U., and Snipes, J.C. (1995). Biology and genetics of hereditary motor and sensory neuropathies. Annu. Rev. Neurosci. *18*, 45–75.

Suter, U., Snipes, G.J., Schoener-Scott, R., Welcher, A.A., Pareek, S., Lupski, J.R., Murphy, R.A., Shooter, E.M., and Patel, P.I. (1994). Regulation of tissue-specific expression of alternative peripheral myelin protein-22 (PMP22) gene transcripts by two promoter. J. Biol. Chem. *269*, 25795–25808.

Tanaka, J., and Sobue, K. (1994). Localization and charcaterization of gelsolin in nervous tissues: gelsolin is specifically enriched in myelin-forming cells. J. Neurosci. *14*, 1038–1052.

Taylor, V., and Suter, U. (1996). Epithelial membrane protein-2 and epithelial membrane protein-3: Two novel members of the peripheral myelin protein 22 gene family. Gene *175*, 115–120.

Taylor, V., Welcher, A.A., Program, A.E., and Suter, U. (1995). Epithelial membrane protein-1, peripheral myelin protein 22, and lens membrane protein 20 define a novel gene family. J. Biol. Chem. *270*, 28824–28833.

Timmerman, V., *et al*. (1992). The peripheral myelin protein gene PMP22 is contained within the Charcot-Marie-Tooth disease type 1A duplication. Nat. Genet. *1*, 171–175.

Valentijn, L.J., Baas, F., Wolterman, R.A., Hoogendijk, J.E., van den Bosch, N.H.A., Zorn, I., Gabreels-Festen, W.M., de Visser, M., and Bolhuis, P.A. (1992a). Identical point mutations of PMP-22 in Trembler-J mouse and Charcot-Marie-Tooth disease type 1A. Nat. Genet. *2*, 288–291.

Valentijn, L.J., *et al*. (1992b). The peripheral myelin gene PMP-22/GAS-3 is duplicated in Charcot-Marie-Tooth disease type 1A. Nat. Genet. *1*, 166–170.

Van Aelst, L., and D'Souza-Schorey, C. (1997). Rho GTPase and signaling network. Genes & Dev. *11*, 2295–2322.

Welcher, A.A., Suter, U., De Leon, M., Snipes, G.J., and Shooter, E.M. (1991). A myelin protein is encoded by the homologue of a growth arrest-specific gene. Proc. Natl. Acad. Sci. USA *88*, 7195–7199.

Wennstrom, S., Hawkins, P., Cooke, F., Hara, K., Yonezawa, K., Kasuga, M., Jackson, T., Claesson, W.L., and Stephens, L. (1994). Activation of phosphoinositide 3-kinase is required for PDGF stimulated membrane ruffling. Curr. Biol. *4*, 385–393.

Xue, D., and Horvitz, R.H. (1995). Inhibition of the *Caenorhabditis elegans* cell-death protease CED-3 by a CED-3 cleavage site in baculovirus p35 protein. Nature *377*, 248–251.

Zoidl, G., Blass-Kampann, S., D'Urso, D., Schmalenbach, C., and Muller, H.W. (1995). Retroviral-mediated gene transfer of the peripheral myelin protein PMP22 in Schwann cells: modulation of cell growth. EMBO J. *14*, 1122–1128.

Zoidl, G., D'Urso, D., Blass-Kampamann, S., Schmalenbach, C., Kuhn, R., and Muller, H.W. (1997). Influence of elevated expression of rat wild-type PMP22 and its mutant PMP22Trembler on cell growth of NIH3T3 fibroblasts. Cell Tissue Res. *287*, 459–470.